ISSN 1063-7729, Astronomy Reports, 2016, Vol. 60, No. 11, pp. 971–995. © Pleiades Publishing, Ltd., 2016.
Original Russian Text © T.S. Khruzina, I.B. Voloshina, V.G. Metlov, 2016, published in Astronomicheskii Zhurnal, 2016, Vol. 93, No. 11, pp. 942–967.

A Photometric Study of the Eclipsing Dwarf Nova GY Cnc in Quiescence and during an Outburst

T. S. Khruzina[1*], I. B. Voloshina[1], and V. G. Metlov[1,2]**

[1] *Sternberg Astronomical Institute, Moscow State University, Universitetskii pr. 13, Moscow, 119991 Russia*

[2] *Crimean Astronomical Station, Moscow State University, Nauchnyi, Russia*

Received April 21, 2016; in final form, June 17, 2016

Abstract—The results of photometric observations of the dwarf nova GY Cnc in the Rc filter acquired in 2013–2015 (∼3900 orbital cycles, 19 nights in total) are presented, including observations during its outburst in April 2014. The binary's orbital elements have been refined. The orbital period has changed only insignificantly during the $\sim 30\,000 P_{\rm orb}$ since the earlier observations; no systematic O–C variations were detected, only fluctuations within 0.004^d on time scales of $1500{-}2000 P_{\rm orb}$. A "combined" model is used to solve for the parameters of GY Cnc during two states of the system. The flux from the white dwarf is negligible due to the star's small size. The temperature of the donor star, $T_2 \sim 3667$ K (Sp M0.2 V), varies between 3440 and 3900 K (Sp K8.8–M1.7 V). The semi-major axis of the disk is $a \sim 0.22a_0$, on average. In quiescence, a varies within ∼40%. The disk has a considerable eccentricity ($e \sim 0.2{-}0.3$) for $a \lesssim 0.2a_0$. The disk shape becomes more circular ($e < 0.1$) with increasing a. The outburst of GY Cnc was associated with increased luminosity of the disk due to the parameter α_g (related to the viscosity of the disk material) decreasing to 0.1–0.2 and the temperature in the inner parts of the disk increasing twofold, to $T_{\rm in} \sim 95\,000$ K. These changes were apparently due to the infall of matter onto the surface of the white dwarf as the outburst developed. All parameters of the accretion disk in quiescence display considerable variations about their mean values.

DOI: 10.1134/S1063772916110020

1. INTRODUCTION

Cataclysmic variables (CVs) are low-mass binaries in the second mass-transfer stage. They consist of a late-type secondary, or donor, star that overflows its Roche lobe, with this material being transferred to a degenerate white-dwarf (WD) or brown-dwarf companion. In dwarf novae without a magnetic field, the transferred matter creates an accretion disk around the WD, enabling matter to accrete on the WD surface. The mean mass-transfer rate varies within a wide range, resulting in CVs of different types.

Dwarf novae (DNe) are one type of CV. Sudden outbursts happen from time to time, against the background of a relatively quiescent state. It is generally believed that the instability that leads to the outbursts appears when the amount of matter accumulated in the accretion disk reaches a critical value. Due to thermal instability, the viscosity of the matter changes abruptly, and the rate of matter transfer in the disk increases considerably. Since the disk luminosity is proportional to the accretion rate, the radiation flux from the disk increases by a factor of 10–1000, depending on the system parameters, initiating the DN outburst.

The orbital periods of DNe range from ∼80 minutes to ∼12 hours. The period distribution of CVs displays a deficiency of objects of 2–3 h—the so-called period gap. Along with their normal outbursts, DNe with periods below the period gap exhibit superoutbursts and "superhumps" in the system's light curve. This subclass of DNe is called SU UMa variables. DNe with periods that are considerably longer than gap periods have different typical characteristics, and are classified as U Gem (classical systems) or Z Cam DNe (stars of the latter type exhibit so-called "standstills", a transitional state between quiescence and outburst). For a detailed review of DNe, see [1].

It is possible to determine the physical characteristics of an eclipsing-CV binary system (orbital inclination, component mass ratio, component temperatures, accretion-disk size, character of the radial temperature variations in the disk) because of the high sensitivity of the eclipse profile to the component parameters. For example, it was established that the

*E-mail: kts@sai.msu.ru
**E-mail: vib@sai.msu.ru

disk radius influences the depth of the eclipse profile, while the parameter α_g in the formula for the radial temperature distribution in the disk, $T(r) \sim r^{-\alpha_g}$, influences the profile shape at the eclipse ingress and egress: the higher the temperature gradient, the smoother the eclipse wings [2]. Among CVs, DNe provide the best possibility for studies of changes of the disk structure in the case of a varying accretion rate.

The aim of the current study is to analyze high-accuracy photometric observations of the DN GY Cnc, plot detailed light curves for the system's active and quiescent states during 2013–2015, investigate the brightness variations for both states and to clarify the nature of these variations, determine the system parameters applying a "combined" CV model, and compare synthetic and observed light curves.

Section 2 briefly describes the GY Cnc system and observational results obtained earlier. Sections 3 and 4 describe our observations and the light-curve shape. Section 5 introduces the orbital elements used to compute the phases for our observations. Section 6 briefly describes the CV model used to search for the parameters of GY Cnc, and the parameter values derived for various epochs are given in Section 7. Sections 8 and 9 discuss and summarize the results obtained.

2. BRIEF INFORMATION ABOUT THE SYSTEM

The system GY Cnc = GSC 1404.1830 = USNO-A2.0 1050-05975509 = HS 0907+1902 = J0909+1849 (RX, 1RXS) was detected in the Hamburg Schmidt objective prism survey [3]; the system is a bright X-ray source in the 0.1–2.4 keV range in the ROSAT Bright Source Catalogue of 1990–1991 [4]. The star was identified as a possible CV in [5]. From further photometry and spectroscopy [6], the object was identified as an eclipsing DN with an orbital period of about 4 h. Shafter et al. [2] detected various brightness states of the system, thus confirming the object's classification as a CV. They used eclipse profiles to determine the temperatures of the WD, hot spot, and accretion disk, and noted that their dependent on the component mass ratio q was weak. Estimates of the main parameters were obtained in [7]: $q = M_{\rm wd}/M_2 = 2.44 \pm 0.25$, $i = 77.0° \pm 0.9°$. Observations outside eclipses were not taken into account in [2, 7]; the profile is already asymmetric at the eclipse egress, and cannot be described in this parametric model [2].

Kato et al. [8] used VSNET data in the Rc filter obtained on an outburst descending branch and in quiescence to estimate the typical time interval between the outbursts as 200–300 days. This is the longest recurrence time among DNe with similar orbital periods. The fading was nearly linear during the outburst egress, at a mean rate of 0.65^m/day. Studies of eclipse profiles in the light curves of GY Cnc obtained on the descending branch of outbursts reveals increasing asymmetry and a systematic decrease of the eclipse width. Light curves with a missing pre-eclipse hump are often observed—a possible consequence of a low hot-spot temperature due to a lower mass-transfer rate between the components, compared to typical CVs.

A statistical study of the outburst activity of GY Cnc based on photographic material from the Sonneberg Observatory (about 18 outbursts) [9] demonstrates that the mean duration of the outbursts is $\sim 5^d$. The brightness at maximum can reach 12.5^m; a plateau with a duration of $\sim 2^d$ is observed at the 14^m level. The out-of-eclipse flux from the system in quiescence is $V \sim 16^m$.

The spectrum of GY Cnc is typical of a DN in its non-active state. The spectral type of the secondary, M3±1.5 V [6], was estimated by comparing its spectrum to data from a catalog of observed M-dwarf spectra. A similar result but with lower uncertainty was obtained in [7]: M3±0.5 V. The radial-velocity curves have semi-amplitudes $K_2 = 297 \pm 15$ and $K_1 = 115 \pm 7$ km/s [7], giving the component mass ratio $q = M_{\rm wd}/M_2 = 2.6 \pm 0.3$. However, taking into account possible distortion of lines could potentially decrease this ratio to $q \sim 1.5$ [7].

Table 1 presents various parameters of GY Cnc determined applying a parametric eclipse model with various assumptions about the structure of the system. However, these system parameters are not very reliable, due to the observed variations of the shape of the GY CnC light curve from cycle to cycle, including variations of the eclipse profile itself. We accordingly attempted to refine the basic parameters of GY Cnc using a "combined" CV model taking into account not only the eclipse region but the entire light curve of the system.

3. OBSERVATIONS

We observed GY Cnc using CCD photometers installed at the 50- and 60-cm telescopes of the Sternberg Astronomical Institute's Crimean Astronomical Station. The light detector used with the 50-cm telescope was an Apogee Alta U8300 CCD camera (3326 × 2504 pixels, 1 pixel = 5.4 μm), with a sensitivity maximum of 60% in the 5800–6600 Å range and 30% at ∼4000 Å. We used an Apogee 47 CCD camera (1024 × 1024 pixels, 1 pixel = 13 μm) with the 60-cm telescope. The duration of our sets of observations depended on the weather, 5–6 h, on

Table 1. Parameters of GY Cnc derived from the eclipse profile analysis and spectroscopic observations

Parameter	Value	Reference	Parameter	Value	Reference
i, deg	73–79 77.3 ± 0.9	[6] [7]	a_0, $R_\odot$	1.30–1.55	[6]
$q = M_{\rm wd}/M_2$	1.4–3.3 2.6	[6] [7]	ξ, a_0	0.54–0.62	[6]
$M_{\rm wd}$, $M_\odot$	0.56–1.25 0.99 ± 0.12	[6] [7]	K_1, km/s	297 ± 15	[7]
M_2, $M_\odot$	0.39–0.37 0.38 ± 0.06	[6] [7]	K_2, km/s	115 ± 7	[7]
$R_{\rm wd}$, $R_\odot$	(13.1–5.1) $\times 10^{-3}$	[6]	R_d, a_0	0.27–0.37	[6]
$R_{\rm wd}$, a_0	0.0100–0.0033	[6]	R_d, ξ	0.5–0.6	[2]
R_2, $R_\odot$	0.43–0.45	[6]	d, pc	320 ± 100 200–250	[6] [2]
$T_{\rm wd}$, K	20000–80000	[6]	$(B-V)$	0.46–0.48 0.45 ± 0.07	[6] [2]
T_2, K	3370–3480	[6]	Sp	M3 $\pm$ 0.5 V M3–4 V	[6] [2]

a_0 is the distance between the component centers of mass; K_1 the radial-velocity amplitude of the WD; K_2 the radial-velocity amplitude of the secondary; d the distance to the system; and ξ the distance between the component centers of mass.

average. The duration of a single exposure with the 60-cm telescope was 60 s; the exposures on the 50-cm telescope were 40–90 s, depending on the weather conditions and the object's brightness. Our observations were performed in the red, in the Rc band, which is close to the Johnson R band, because the sensitivity of the CCD detector used is highest in the red. The uncertainty of a single observation depended on the weather, and was approximately the same for both telescopes, $\sigma(i) \sim 0.02{-}0.06^m$.

The comparison star was Star 137 from the AAVSO list of standards; this star lies in the nearest vicinity of GY Cnc, and has coordinates $\alpha(2000) = 9^{\rm h}09^{\rm m}57\overset{\rm s}{.}8$ and $\delta(2000) = +18°49'03''$, with $V = 13.740^m$ and $Rc = 13.665^m$. We checked for constancy of the brightness of the standard star using several check stars. We reduced our observations applying the aperture photometry technique using the MAXIM-DL software package.

Our monitoring of GY Cnc began in October 2013, and is currently still ongoing. We analyzed observations taken in 2013–2015. A log of the observations used in our analysis is presented in Table 2. Figure 1 displays the time distribution of the observations obtained. The bulk of our observations correspond to the system's quiescence. We observed a single outburst (April 14–21, 2014), though the brightness level of the data for April 20 and April 21 already indicate a transition of the system to its non-active state.

4. LIGHT CURVES OF GY Cnc

Figure 2 displays the unaveraged light curves of the binary GY Cnc obtained in 2013–2015 on the same scale. For convenience, we have labeled each observing run with the last four digits of its Julian date; the fractions of the corresponding Julian day are plotted along the horizontal axis. The considerable variations of the light curve shape and of the system's minimum eclipse brightness in quiescence, which varies between 16.8^m and 17.2^m, are obvious. The variation amplitude changes from 0.8^m to 1.2^m, with the lowest amplitude being due to the binary's lower out-of-eclipse brightness, with the eclipse remaining at a level of $17.1{-}17.2^m$ (JD 7107, JD 7108).

Figure 3 shows the evolution of the GY Cnc light curve during the outburst in April 2014. The observations during the actual outburst are those on JD 6762–6764, when the out-of-eclipse brightness of the system increased to $\sim 13^m$. Though the observations on JD 6768–6769 are fairly close to the outburst time, $\Delta t \sim 4^d$, the level of the out-of-eclipse brightness and light-curve shape indicate that they should be attributed to quiescence. In agreement with the conclusions of Shugarov et al. [9], after a rapid ($\sim 1^d$) flux rise to a maximum, the outburst reached

Table 2. Log of observations of the binary GY Cnc in 2013–2015

Date	T_1, T_2, JD2450000+	Phases, $\varphi_1-\varphi_2^*$	N	$T_{\min}$ (obs.) JD2450000+	$T_{\min}$ (theor.) JD2450000+	$Rc_{\min}$	$Rc_{\max}$
2013.12.18	6645.329, 6645.542	0.356–1.571	255	6645.443691	6645.441450	17.10	15.86
2013.12.20	6647.307, 6647.474	0.627–1.583	198	6647.371737	6647.371185	16.96	15.75
2013.12.23	6650.362, 6650.652	0.058–1.710	349	6650.527210	6650.527034	16.96	15.81
2014.02.02	6691.202, 6691.455	0.830–2.272	217	6691.231377 6691.407222	6691.405368	17.07	16.00
2014.02.03	6692.175, 6692.475	0.373–2.085	364	6692.284844 6692.460275	6692.282579	17.14	15.95
2014.02.04	6693.213, 6693.460	0.302–1.707	212	6693.335983	6693.335142	17.12	16.09
2014.02.05	6694.363, 6694.535	0.854–1.837	205	6694.388703	6694.387359	16.95	15.91
2014.03.24	6741.217, 6741.458	0.905–2.276	287	6741.234028 6741.407604	6741.231137	16.95	15.83
2014.03.31	6748.211, 6748.477	0.770–2.284	323	6748.252094 6748.426228	6748.250617	17.09	16.01
Outburst 2014.04.14	6762.221, 6762.474	0.620–2.061	447	6762.286921 6762.463414	6762.463307	14.49	12.94
Outburst 2014.04.16	6764.268, 6764.416	0.284–1.127	248	6764.394039	6764.393471	16.23	13.82
Outburst 2014.04.20	6768.238, 6768.438	0.912–2.054	246	6768.251134 6768.428912	6768.428188	17.04	15.68
Outburst 2014.04.21	6769.280, 6769.440	0.854–1.771	194	6769.305601	6769.305532	16.89	15.67
2014.05.02	6780.246, 6780.397	0.342–1.198	181	6780.362234	6780.359053	16.84	15.87
2014.05.07	6785.245, 6785.394	0.844–1.694	175	6785.272824	6785.271635	16.86	15.74
2015.03.25	7107.287, 7107.499	0.470–1.676	279	7107.380694	7107.379369	17.23	16.30
2015.03.26	7108.228, 7108.470	0.831–2.113	285	7108.257615 7108.434722	7108.256125	17.10	16.33
2015.11.04	7331.425, 7331.628	0.998–2.153	200	7331.425462 7331.601238	7331.599876	17.18	15.94
2015.11.05	7332.417, 7332.633	0.674–1.902	197	7332.474618	7332.474586	17.24	15.94

* The ephemeris (1) was used to calculate the phases at the beginning and end of our observations, φ_1 and φ_2. $T_{\min}$(theor.) corresponds to the time of mid-eclipse of the WD computed in the process of finding the solution.

a plateau lasting $\sim 2^d$. The time for a decrease by $\sim 1^m$ is ~ 2–4^d; the brightness behavior below 14^m is unknown. Our data demonstrate that the system's brightness had already returned to its normal level six days after the maximum (JD 6762).

Six of the 19 observing runs were obtained with the 50-cm AZT-5 telescope, and the remaining 13 runs with the 60-cm Zeiss-600 telescope. To get a uniform data set, we observed GY Cnc simultaneously with the two telescopes on two nights. A comparison of the resulting light curves indicated that, in order to reduce the observations performed

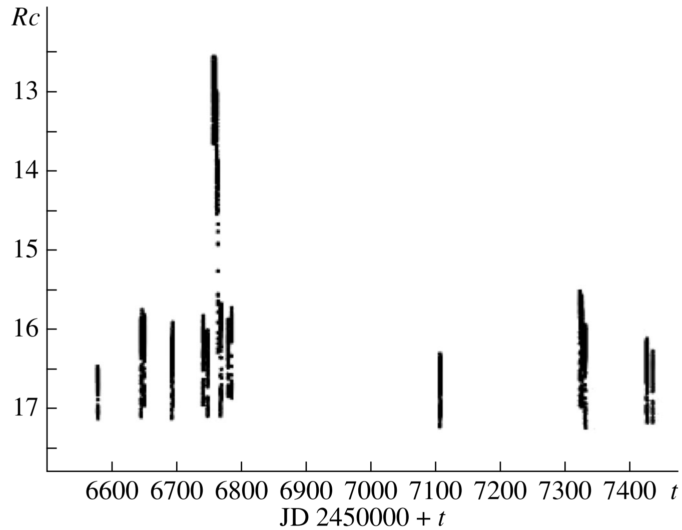

Fig. 1. Time distribution of our observations of GY Cnc.

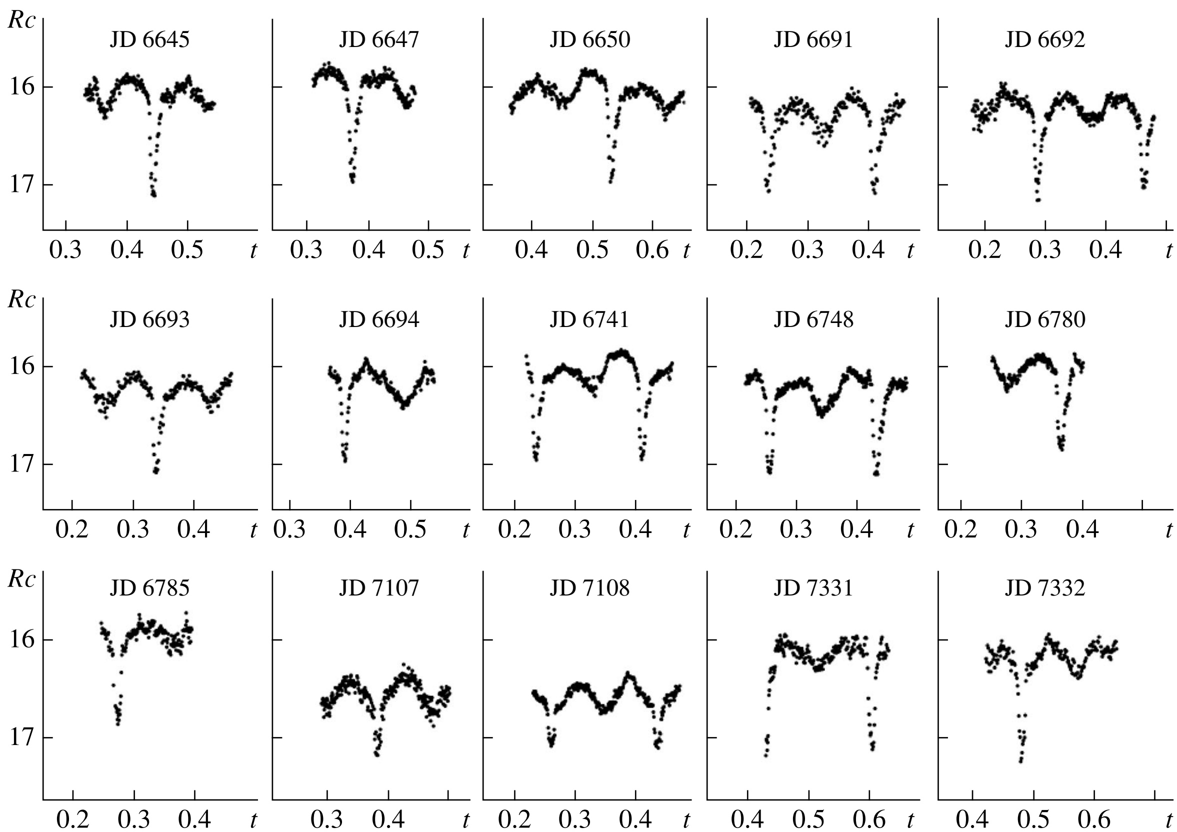

Fig. 2. Light curves of GY Cnc observed in 2013–2015 during quiescence.

with the 50-cm telescope ($Rc50$) to the 60-cm instrumental system ($Rc60$), a magnitude correction $Rc60 = Rc50 - 0.05^m$ is needed. As an example, Fig. 4 displays the light curves of GY Cnc obtained with the two telescopes on February 3, 2014 (JD 6692): the gray circles show data from the 60-cm telescope and the black circles data from the 50-cm telescopes. The curves are similar in their overlapping parts. All the light curves presented in Figs. 2 and 3 are in the 60-cm instrumental system.

Unfortunately, several observing runs obtained on October 27–31, 2015 cover the orbital period in-

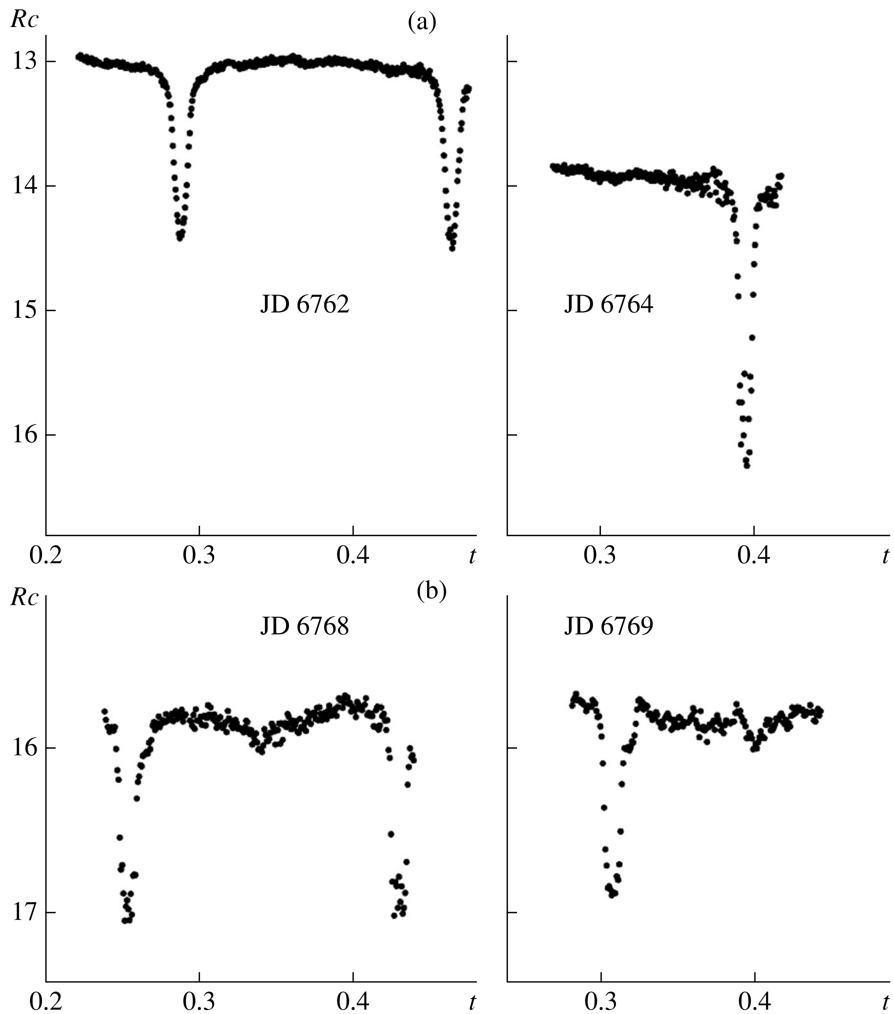

Fig. 3. Observations of GY Cnc obtained during the outburst (a) and six and seven days after the observed brightness maximum (b).

completely, and we accordingly did not use them in our susequent computations or include them in Table 2. Though incomplete, these light curves (see Fig. 5) clearly demonstrate that the system's quiescence light curve continuously changes: the magnitude at the minimum is approximately the same on the first three nights, $\sim 17^m$, and the out-of-eclipse brightness level was decreasing by $\sim 0.2-0.3^m$/day; on the fourth night, the out-of-eclipse part of the light curves was distorted, with fluctuations having a semi-amplitude of up to $\sim 0.2^m$, which became a factor of two lower on the fifth night. Similar fluctuations are also visible on other nights (see Figs. 2, 3), in both the active and quiescent states.

5. ORBITAL EPHEMERIDES

All the ephemerides available for GY Cnc up until now were based on observations obtained in 2000. Table 3 contains the epoch of minimum brightness in the light curve ($T_{\min}$), the orbital period ($P_{\rm orb}$) in days for this epoch, references, the O–C deviation in days, and the number of complete orbital cycles N elapsed from the first primary minimum in our observations, JD 2456645.44145.

Our observations were obtained more than 10 years after the observations on which the binary's orbital ephemerides were based. We performed our own search for the orbital period of GY Cnc, using only our 2013–2015 observations. To compute the power spectra, we used a code written and provided by V.P. Goranskij, based on the Lafler–Kinman technique. We searched for the orbital period in 2013–2015 using uniform observations (without outbursts) in the range $0.1753-0.1756^d$ in steps of 0.000001^d. The resulting power spectra are shown in Fig. 6 with two different frequency resolutions.

Within the uncertainties, the maximum in the power spectrum corresponds to the periods deter-

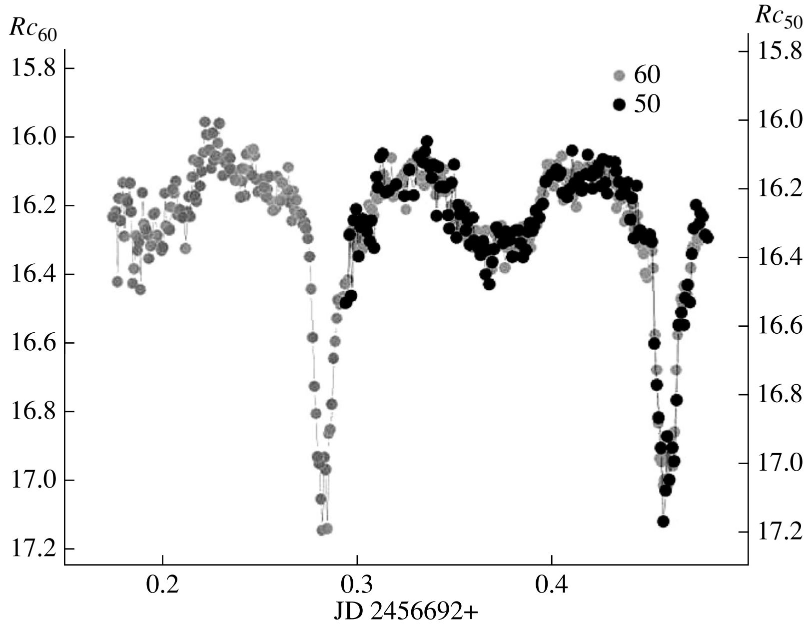

Fig. 4. Light curves of GY Cnc obtained on February 3, 2014 (JD 6692) with the 60-cm (gray circles) and 50-cm (black circles) telescopes.

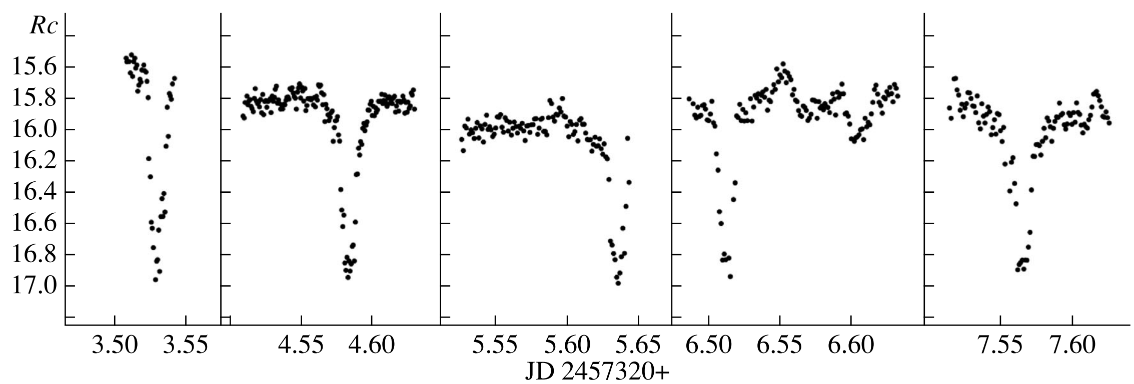

Fig. 5. Observations of GY Cnc on five successive nights (October 27–31, 2015) that were not used in our subsequent analysis due to incomplete coverage of the orbital cycle.

mined in [2, 8, 10].

$$T_{\min} = 2456645.44145(6) + 0.1754420(8)^d N. \quad (1)$$

We took the time of the WD's mid-eclipse from the solution for the close binary's parameters determined from the light curve observed on the first night of our observations, JD 6645, as the zero epoch. The technique used to calculate the refined epoch of the brightness minimum is described in [11]. The column $T_{\min}$(theor.) in Table 2 contains the epochs of the WD's mid-eclipse calculated in this way for the corresponding orbital cycles. The O–C deviations between the "refined" epochs of minima and those calculated from the ephemeris (1) are displayed in Fig. 7. Here, we do not present data 2000 from Table 3, which consist of only three data points with $N \sim -28\,862$, $-28\,837$, and $-28\,532$ and have approximately the same deviation, O–C $\sim 0.043–0.046$ (see Table 3). The arrow marks the data points corresponding to the outburst in April 2014. Evidently, the outburst did not change the current O–C value. The closeness of the derived period to the values determined at a time $\sim 28\,000 P_{\text{orb}}$ earlier, within the uncertainties, indicates an absence of systematic period variations. The data instead suggest O–C fluctuations within $\sim 0.004^d$.

Figure 8 presents all the observations of GY Cnc folded with the orbital ephemeris (1). This plot shows a large dispersion of the data points along the entire orbital light curve, both in and out of eclipse, with

Table 3. Ephemerides of GY Cnc from observations of 2000 and 2013–2015

$T_{\rm min}$	$P_{\rm orb}$, days	Reference	O–C, days	N
		Quiescence		
2451581.8263(1)	0.175446(3)	[6]	+0.0464	−28 862
2451581.8265(1)	0.175441(1)	[2]	+0.0453	−28 862
2451639.7228	0.175444	[7]	+0.0428	−28 532
2451581.82665(1)	0.175442499(2)	[10]	+0.0444	−28 862
2451586.21271(8)	0.17544251(5)	[8]	+0.0444	−28 837
2456645.44145(6)	0.1754420(8)	This paper	−0.01370–+0.0272	0–3916
		Outburst		
2456762–6769	0.1754420(8)	This paper	+0.0116–+0.0134	667–706

N is the number of orbital cycles elapsed since JD 2456645.44145.

an apparent separation into three typical curves. The bottom curve displays dominating ellipsoidal variations of the secondary, with a small contribution by light from the disk, and possibly also the region where the gas stream collides with it, with the eclipse of these regions reflected by a shallow minimum. The pre-eclipse hump is completely missing here. The second and third typical curves have higher out-of-eclipse brightness levels, by $\sim 0.3^m$ and $\sim 0.6^m$ and an obvious pre-eclipse hump ($\Delta Rc \sim 0.1^m$); the depth of the eclipse varies less change than the out-of-eclipse brightness. Below, we consider the parameters of the system whose variations result in this large scatter in the observational data and the stratification of the light curves.

6. MODEL OF THE SYSTEM

To determine the parameters of GY Cnc in the orbital cycles observed in 2013–2015 during the different activity states, we used smoothed light curves for the system, with each normal point obtained by averaging a sequence of 5–20 observations in a phase interval $\Delta\varphi \sim 0.02-0.03$. We averaged observations in the region of the primary minimum only if there were two or more observations within $\Delta\varphi \simeq 0.01$. In other cases, an unaveraged observation was taken as a normal point. We took the uncertainties to be the mean uncertainty of a single observation in the set, $\sim 0.02-0.04^m$.

We solved for the system's parameters using the "combined" CV model described in detail in [12, 13], whose main features are outlined briefly below.

6.1. Main Features of the Model

The system consists of a WD surrounded by a disk and a red dwarf (RD) that completely fills its Roche lobe. The RD is subdivided into 648 area elements, each radiating in accordance with its own effective temperature T_i that depends on the effective temperature of the secondary, T_2. When computing T_i, we took into account heating of the RD surface by radiation from inner regions of the accretion disk with the temperature $T_{\rm in}$, $T_{\rm in} \geq T_{\rm wd}$, where $T_{\rm wd}$ is the temperature of the WD. The shape and size of the secondary are determined by the parameter $q = M_{\rm wd}/M_2$; the RD fills its Roche lobe completely. Our computations of the fluxes from the area elements on the RD surface took into account gravitational darkening and limb darkening in a non-linear approximation.

The WD is represented with a sphere with the radius $R_{\rm wd}$; it is surrounded by a slightly elliptical accretion disk with eccentricity e and semi-major axis a. The disk orientation is described by the angle α_e, which is the angular distance in the orbital plane between the disk's periastron and the line connecting the centers of mass of the components (which we called the system's axis). The disk is optically think and has a complex shape: it is geometrically thin near the surface of the WD and geometrically thick at its outer edge, with opening angle β_d. The temperature of each area element on the disk is expressed by the formula

$$T(r) = T_{\rm in}(R_{\rm in}/r)^{\alpha_g}, \quad (2)$$

where $R_{\rm in}$ is the radius of the first orbit near the WD, $R_{\rm in} \sim R_{\rm wd}$, and the parameter α_g is proportional to the gas viscosity in the disk. If each point of the disk's surface radiates as a blackbody, we have, in a first

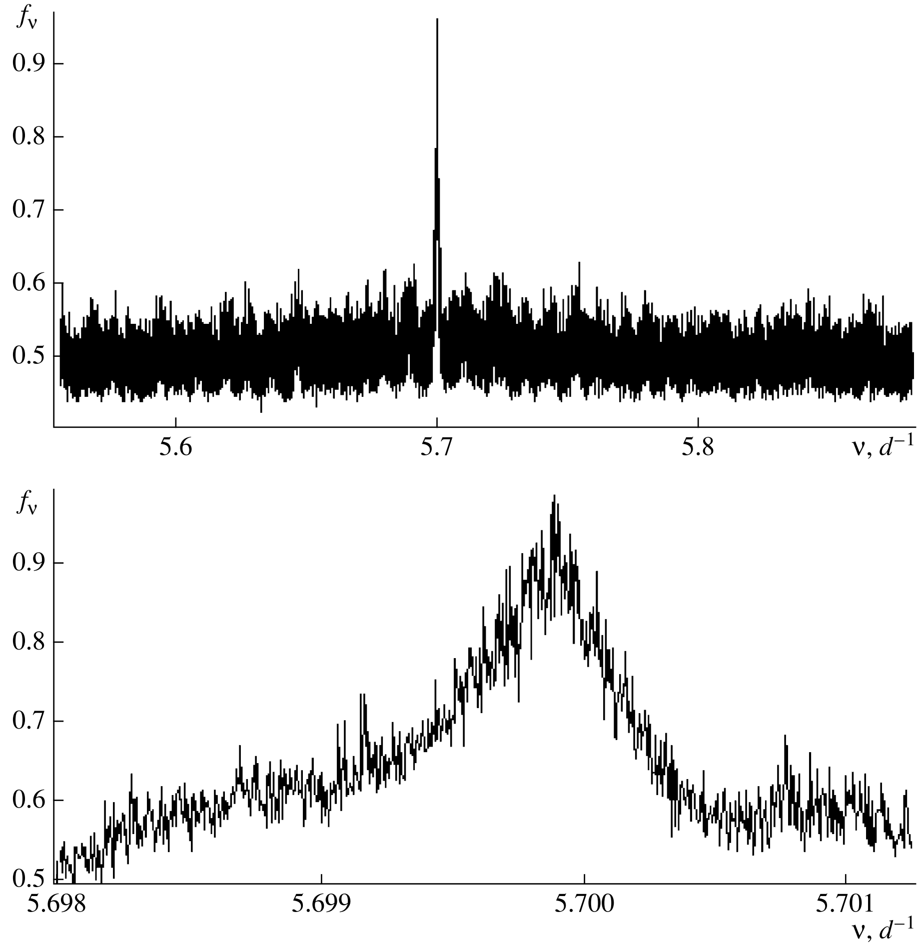

Fig. 6. Lafler–Kinman periodograms with two frequency resolutions for the 2013–2015 observations of GY Cnc.

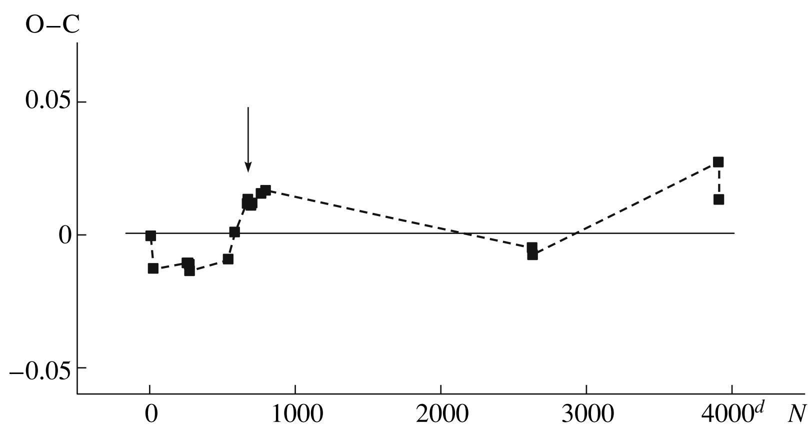

Fig. 7. O–C values for GY Cnc in 2013–2015. The arrow corresponds to the outburst in April 2014.

approximation $\alpha_g = 0.75$ [14]. In the active state of the CV, α_g can decrease to $\sim$0.1, so that the radial temperature distribution in the disk becomes flatter, and the flux from the disk becomes higher for the same $T_{\rm in}$ values. The computations of the local temperature of a selected area element took into account heating by radiation from the secondary (as a rule, this effect is insignificant) and by high-temperature radiation from inner parts of the disk.

Finally, an additional radiating component is the

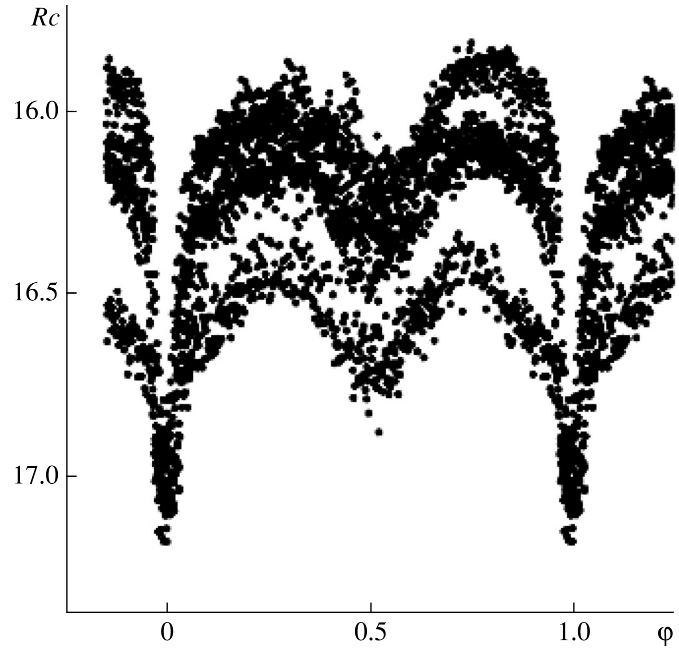

Fig. 8. All observations of GY Cnc in quiescence folded with the orbital ephemeris (1).

region of interaction between the gas stream and the disk's lateral surface. Gas-dynamical studies of the steady pattern of matter flows in semi-detached binaries demonstrate that the interaction between the stream and disk is collisionless (e.g., [15, 16]). A shock is formed, but only in a narrow region along the edge of the stream (the "hot line"), as a result of the interaction of the incoming flows in the disk and circumdisk halo with matter in the stream. As a result, the region of energy release in our model consists of two regions on the surface of the hot line, on its windward and leeward sides, and a hot region on the lateral surface of the disk. The radiating region of the hot line is reproduced as a truncated ellipsoid, with its center located in the orbital plane inside the disk, while the hot spot is modeled as a half ellipse on the lateral surface of the disk, to the leeward side of the stream. The center U of this ellipse coincides with the intersection of the axis of the gas stream with the disk (see [13] for more details).

The main parameters of the interaction region between the gas stream and the lateral surface of the disk are: (1) the semi-axes a_v, b_v, and c_v of the truncated ellipsoid describing the hot line; (2) the highest temperatures of the stream material at the boundary of the disk, on the windward ($T_{ww,\max}$) and leeward ($T_{lw,\max}$) sides of the ellipsoid (the temperature of the matter decreases according to a cosine law with increasing distance from the disk edge); (3) the angle β_1 between the axis of the gas stream and the system's axis; and (4) the radius of the hot spot on the lateral surface of the disk, $R_{\rm sp}$ (the distance between the point U and the outer edge of the spot in the orbital plane). Since part of the hot spot is covered by the gas stream, its actual size on the disk surface is smaller, but the covering of part of the spot is compensated by radiating regions on the leeward side of the stream. The parameter $\beta_{\rm sp}$ gives the thickness of the outer edge of the disk (in degrees) in the region of its interaction with the stream. This parameter is usually larger than the thickness of the disk's outer edge in other regions.

The blackbody radiation of all the components is a sum of the fluxes F_j from the area elements into which the system's components were subdivided that are observable at the given orbital phase; we computed the fluxes $F_j(T_i)$ using a Planck formula for the effective temperatures T_i of each of the area elements.

6.2. Scheme for Deriving Best-fit Parameters of the System

We used the Nelder–Mead method [17] to solve for the system parameters that best match the shapes of the synthetic and observed light curve. Searching for the global minimum of the residuals for each of the light curves, we used several dozen different initial approximations, since several local minima are usually present in the studied parameter domain when there are a large number of independent variables. We estimated the agreement between the theoretical and observed close-binary light curves in the framework of our model by calculating the fit residuals

$$\chi^2 = \sum_{j=1}^{n} \frac{(m_j^{\text{theor}} - m_j^{\text{obs}})^2}{\sigma_j^2}, \tag{3}$$

where m_j^{theor} and m_j^{obs} are the theoretical and observed magnitudes of the object at orbital phase j, σ_j^2 is the dispersion of observations at point j, and n is the number of normal points in the curve.

Since the number of free parameters is large, it is necessary to take into account additional information on the system in order to fix some of the problem's parameters during the solution, and thereby to considerably narrow the range of variation of the other parameters.

We solved for a sequence of uniform (i.e., obtained with the same comparison star) light curves of GY Cnc; the difference introduced by the use of different telescopes was eliminated during the data reduction (see Section 3). This enabled us to impose an additional restriction on the region of permitted parameters of the problem. Namely, when a series of several uniform light curves was present, we used the same energy unit to transform the fluxes of our synthetic light curves into magnitudes—the flux from the system at an orbital phase near quadrature, $F_{\text{opt}}(Rc)$, for the curve with the lowest out-of-eclipse brightness. This approach makes it possible to compare the synthetic and observed light curves using both their shape and the flux variations (see, for instance, [18, 19]).

Our search for the solutions consisted of several stages.

The aim of the first stage was to find the energy unit and to select several parameters whose values could be fixed when determining the other parameters of the model. These were usually basic parameters of the system, such as the component mass ratio q, the orbital inclination i, the temperature T_{wd} and radius R_{wd} of the WD, and sometimes the temperature of the secondary. We selected one to two light curves with the lowest contribution from the disk and the neighboring region of energy release and used the Nelder–Mead method to search for the parameters providing a synthetic light curve that best fit the observed one. At this stage, we translated the calculated fluxes into magnitudes using the flux of a given test curve at the first quadrature ($\varphi = 0.25$; $\varphi = 0.0$ corresponds to the upper conjunction of the WD). For this purpose, we selected the quiescence light curves for JD 7107 and JD 7108 (see Fig. 2), which display the lowest out-of-eclipse flux among all the light curves, as well as an obvious dominance of the contribution of the secondary to the combined brightness, with the contribution from the disk being obviously low.

Figure 9 presents the relation between the residual χ^2 and q for these two dates. To enable a comparison of the residuals for two different light curves, we normalized them to the minimum χ^2_{min} for the corresponding run. In the course of a run, we searched for a solution with a fixed value of q in the range $q = 1.3{-}3.3$ obtained in [6, 7] from an analysis of the primary eclipse's shape. All other model parameters were kept free, and were restricted only with their natural variation limits. It follows from the figure that the $\chi^2(q)$ relation for JD 7108 has a minimum near $q \sim 1.7{-}2.4$ (at $\chi^2/\chi^2_{\text{min}} \sim 1.02$). The shape of the $\chi^2(q)$ curve for JD 7107 is considerably narrower, $q \sim 1.7{-}2.15$ even at $\chi^2/\chi^2_{\text{min}} \sim 1.10$, with a minimum at $q \simeq 1.9$. The values of i, R_{wd}, T_{wd}, and $F_{\text{opt}}(Rc)$ corresponding to $q \sim 1.7{-}2.2$ are distributed in the following ranges: $i \sim 71.6^\circ{-}74.3^\circ$, $R_{\text{wd}}/\xi \sim 0.0068{-}0.0073$, $T_{\text{wd}} \sim 16\,040{-}19\,020$ K, and $F_{\text{opt}} \sim (0.097{-}0.110) \times 10^{-9}$ rel. units for $Rc = 15.9^m$. Our use of relative units is due to the fact that the Planck function we used to compute the fluxes from the area elements on the system's components per unit wavelength interval is the energy flux passing through an area of 1 cm^2, while the unit distance in the computational code is a_0, the distance between the close-binary components, whose value is not known a priori.

Further, we searched for the parameters using all 13 of the other light curves in quiescence, with the range of the basic parameters restricted to the above limits. Based on the results, we fixed the basic parameters at the following average values: $q = 1.9$, $i = 73.0^\circ$, $R_{\text{wd}} = 0.007\xi$, $T_{\text{wd}} = 17\,490$ K, and $F_{\text{opt}} = 0.106 \times 10^{-9}$ rel. units for $Rc = 15.9^m$. Note that, although the system's spectral type determined from the observations of [6, 7] is M (3 ± 1.5) V, corresponding to an effective temperature for the secondary $T_2 \sim 3030{-}3480$ K [20], the optimal T_2 values derived at the first stage were often found to be outside this range. Because of this, we did not fix the parameter T_2 in our further computations.

A comparison of our basic parameters to those determined in other studies (Table 1) reveals some differences. This is apparently due to the fact that, in all earlier studies, the system parameters were based only on fits to the region of the eclipse, while we have used the whole light curve for this purpose.

At the second stage, we searched for the best-fit system parameters of GY Cnc for all the light curves, in both quiescence and during the outburst, taking into account the flux normalization to the selected value, $F_{\text{opt}}(Rc)$, and the basic parameters fixed as discussed above. The system parameters derived in the second stage are presented in Table 4, for both

Table 4. Parameters of the DN GY Cnc obtained from an analysis of light curves observed in 2013–2015 assuming $q = M_{\rm wd}/M_2 = 1.9(2)$, $i = 73.0(4)^\circ$, $R_{\rm wd} = 0.0040(7)a_0$, and $T_{\rm wd} = 17\,490 \pm 415$ K. The value $q = 1.9(2)$ corresponds to a mean radius for the secondary $\langle R_2\rangle = 0.335(7)a_0$ and to $\xi = 0.566(14)a_0$

Parameter	JD 2456645	2456647	2456650	2456691	2456692	2456693	2456694
Quiescence							
N accord. to (1)	0	11	29	261	267	273	279
O–C	0	−0.000720	−0.012740	−0.010750	−0.010744	−0.011252	−0.0137310
$Rc_{\max}$	15.86	15.75	15.81	16.00	15.95	16.09	15.91
$Rc_{\min}$	17.10	16.96	16.96	17.07	17.14	17.12	16.95
T_2, K	3514 ± 57	3722 ± 30	3642 ± 30	3790 ± 20	3614 ± 36	3797 ± 16	3867 ± 24
Accretion disk parameters							
e	0.175(11)	0.144(16)	0.040(12)	0.283(23)	0.077(6)	0.192(23)	0.172(44)
R_d(max), ξ	0.329(8)	0.359(25)	0.374(8)	0.294(11)	0.357(4)	0.299(5)	0.29(2)
R_d(min), a_0	0.131(8)	0.152(25)	0.196(8)	0.093(11)	0.173(4)	0.115(5)	0.116(20)
R_d(max), a_0	0.158(8)	0.203(25)	0.212(8)	0.166(11)	0.202(4)	0.169(5)	0.164(20)
a, a_0	0.158(4)	0.177(12)	0.204(5)	0.130(5)	0.188(2)	0.142(2)	0.14(1)
$0.5\beta_d$, deg	2.08(45)	3.06(14)	2.89(14)	1.9(1)	1.76(7)	2.0(1)	2.6(3)
$T_{\rm in}$, K	$40\,830 \pm 740$	$42\,354 \pm 470$	$35\,005 \pm 395$	$41\,840 \pm 930$	$43\,160 \pm 515$	$40\,245 \pm 685$	$34\,980 \pm 570$
$T_{\rm out}$, K	6316 ± 87	7216 ± 51	5860 ± 50	9405 ± 80	5435 ± 58	5050 ± 58	10540 ± 80
α_g	0.548(1)	0.551(5)	0.504(5)	0.665(7)	0.545(2)	0.652(7)	0.520(6)
α_e, deg	93 ± 11	89 ± 4	133 ± 5	115 ± 5	33 ± 9	101 ± 2	37 ± 7
Hot line parameters							
a_v, a_0	0.049(2)	0.065(2)	0.062(1)	0.031(1)	0.046(1)	0.041(1)	0.040(1)
b_v, a_0	0.391(8)	0.381(5)	0.361(9)	0.418(11)	0.331(5)	0.416(5)	0.352(7)
c_v, a_0	0.009(2)	0.012(1)	0.014(1)	0.007(1)	0.008(1)	0.007(1)	0.008(1)
$T_{ww,\max}$, K	$20\,020 \pm 1040$	$22\,990 \pm 905$	$14\,515 \pm 790$	$18\,565 \pm 800$	$20\,210 \pm 1775$	$15\,915 \pm 444$	$25\,635 \pm 1465$
$T_{lw,\max}$, K	$17\,850 \pm 175$	$19\,365 \pm 280$	$14\,770 \pm 370$	$15\,620 \pm 200$	$17\,715 \pm 605$	$14\,480 \pm 170$	$19\,390 \pm 300$
β_1, deg	6.4(2)	6.1(2)	11.0(3)	5.8(1)	9.6(5)	6.4(1)	5.5(3)
Hot spot parameters							
$R_{\rm sp}$, a_0	0.14(2)	0.106(21)	0.202(14)	0.059(1)	0.18(6)	0.116(18)	0.055(1)
$0.5\beta_{\rm sp}$, deg	5.5(5)	5.4(8)	6.7(3)	5.3(1)	2.5(3)	5.2(6)	5.8(4)
χ^2	2739	343	882	294	990	294	1103

Table 4. (Contd.)

Parameter	JD 2456741	2456748	2456762	2456764	2456768	2456769
	Quiescence		Outburst			
N accord. to (1)	546	586	667	678	701	706
O−C	−0.009376	+0.000883	+0.011643	+0.013366	+0.010807	+0.011571
$Rc_{\max}$	15.83	16.01	12.94	13.82	15.68	15.67
$Rc_{\min}$	16.95	17.09	14.49	16.23	17.06	16.89
T_2, K	3620 ± 31	3793 ± 16	2786 ± 715	2689 ± 655	3224 ± 65	3727 ± 50
			Accretion disk parameters			
e	0.024(21)	0.225(26)	0.233(5)	0.341(9)	0.206(5)	0.152(36)
$R_d(\max)$, ξ	0.553(12)	0.468(24)	0.311(2)	0.283(1)	0.334(2)	0.329(15)
$R_d(\min)$, a_0	0.298(12)	0.168(24)	0.110(2)	0.079(1)	0.124(2)	0.137(15)
$R_d(\max)$, a_0	0.313(12)	0.265(24)	0.176(2)	0.160(1)	0.189(2)	0.186(15)
a, a_0	0.305(7)	0.216(11)	0.143(1)	0.119(1)	0.157(2)	0.161(7)
$0.5\beta_d$, deg	2.8(2)	2.3(1)	2.26(9)	0.62(1)	1.90(1)	2.5(3)
$T_{\rm in}$, K	$39\,400 \pm 395$	$38\,420 \pm 430$	$95\,030 \pm 700$	$68\,155 \pm 860$	$39\,940 \pm 420$	$36\,400 \pm 940$
$T_{\rm out}$, K	4615 ± 35	4725 ± 33	$59\,530 \pm 430$	$30\,680 \pm 380$	7940 ± 70	$11\,115 \pm 120$
α_g	0.535(4)	0.599(4)	0.110(3)	0.196(5)	0.479(4)	0.51(1)
α_e, deg	148 ± 36	116 ± 5	166 ± 6	168 ± 1	151 ± 1	127 ± 9
			Hot line parameters			
a_v, a_0	0.050(2)	0.072(2)	0.042(2)	0.059(1)	0.055(1)	0.074(2)
b_v, a_0	0.359(13)	0.395(6)	0.386(11)	0.391(4)	0.411(2)	0.41(8)
c_v, a_0	0.019(2)	0.012(1)	0.009(1)	0.002(1)	0.007(1)	0.010(2)
$T_{ww,\max}$, K	$12\,690 \pm 670$	$14\,385 \pm 460$	$80\,550 \pm 8640$	$46\,214 \pm 3190$	$27\,482 \pm 1040$	$22\,205 \pm 1650$
$T_{lw,\max}$, K	$13\,635 \pm 580$	$13\,605 \pm 160$	$75\,440 \pm 2810$	$41\,540 \pm 790$	$21\,120 \pm 300$	$19\,020 \pm 495$
β_1, deg	24.4(8)	8.5(5)	5.6(8)	3.3(1)	6.5(1)	5.1(2)
			Hot spot parameters			
$R_{\rm sp}$, a_0	0.160(27)	0.212(16)	0.07(2)	0.09(7)	0.10(2)	0.11(4)
$0.5\beta_{\rm sp}$, deg	4.6(6)	4.9(4)	4.8 ± 1.4	1.6(6)	3.7 ± 1.0	5.1 ± 1.1
χ^2	1435	362	1232	1694	537	4679

Table 4. (Contd.)

Parameter	JD 2456780	2456785	2457107	2457108	2457331	2457332
Quiescence						
N accord. to (1)	769	797	2633	2638	3911	3916
O−C	+0.015418	+0.016592	−0.004942	−0.007530	+0.027154	+0.012905
$Rc_{\max}$	15.87	15.74	16.30	16.33	15.94	15.94
$Rc_{\min}$	16.84	16.86	17.23	17.10	17.18	17.24
T_2, K	3582 ± 32	3438 ± 50	3840 ± 10	3896 ± 12	3610 ± 32	3737 ± 27
Accretion disk parameters						
e	0.096(13)	0.184(27)	0.164(7)	0.133(23)	0.182(23)	0.268(2)
R_d(max), ξ	0.590(23)	0.455(20)	0.308(20)	0.322(8)	0.377(7)	0.344(2)
R_d(min), a_0	0.275(23)	0.177(20)	0.125(20)	0.140(8)	0.141(7)	0.112(2)
R_d(max), a_0	0.334(23)	0.258(20)	0.174(20)	0.182(8)	0.213(7)	0.195(2)
a, a_0	0.305(12)	0.218(10)	0.150(1)	0.161(4)	0.181(4)	0.154(1)
$0.5\beta_d$, deg	2.0(2)	2.05(16)	1.83(2)	1.7(1)	2.2(1)	2.8(1)
T_{in}, K	$39\,545 \pm 370$	$39\,510 \pm 395$	$39\,160 \pm 390$	$40\,365 \pm 575$	$37\,040 \pm 460$	$35\,240 \pm 825$
T_{out}, K	4715 ± 35	6185 ± 52	3855 ± 27	3670 ± 37	9230 ± 55	4660 ± 75
α_g	0.525(4)	0.486(3)	0.697(7)	0.700(6)	0.522(4)	0.625(8)
α_e, deg	152 ± 1	114 ± 40	76 ± 3	52 ± 15	119 ± 3	102 ± 1
Hot line parameters						
a_v, a_0	0.045(1)	0.050(4)	0.038(1)	0.030(1)	0.052(1)	0.052(1)
b_v, a_0	0.343(1)	0.373(11)	0.369(2)	0.367(5)	0.391(7)	0.413(1)
c_v, a_0	0.014(1)	0.012(1)	0.007(1)	0.007(1)	0.009(1)	0.009(1)
$T_{ww,\max}$, K	$18\,630 \pm 50$	$19\,530 \pm 1200$	$16\,550 \pm 370$	$15\,540 \pm 540$	$21\,620 \pm 1250$	$19\,385 \pm 640$
$T_{lw,\max}$, K	$16\,050 \pm 15$	$16\,435 \pm 675$	$13\,795 \pm 135$	$13\,310 \pm 120$	$17\,040 \pm 350$	$16\,170 \pm 215$
β_1, deg	24.8(7)	11.2(8)	6.9(2)	10.0(2)	8.3(1)	5.0(2)
Hot spot parameters						
R_{sp}, a_0	0.128(1)	0.116(26)	0.104(30)	0.112(66)	0.084(33)	0.167(30)
$0.5\beta_{\text{sp}}$, deg	3.0(1)	3.9 ± 1.1	4.6(5)	3.7(9)	4.2(6)	4.1(9)
χ^2	499	628	55.7	438	236	260

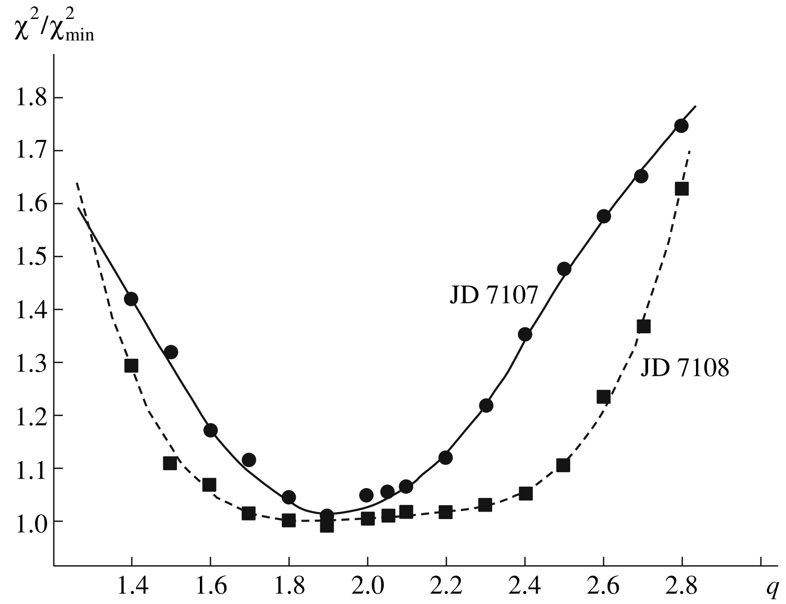

Fig. 9. $\chi^2(q)$ relation obtained when searching by q using two nights of observations, JD 7107 and JD 7108.

quiescence and the active state. The numbers in parantheses are the uncertainties in the one to two last digits of the parameter in question. These uncertainties were obtained via an exhaustive search of the selected parameter until the residual $1.1\chi^2_{\min}$ was achieved, with all other parameters kept at the values providing the minimum residual.

7. MODELING RESULTS

7.1. Light Curves in Quiescence

Figures 10–13 present the theoretical light curves plotted with corresponding parameters from Table 4 for quiescence: for the mean light curves in panel I and for the unaveraged observations in panel II. Panel III displays the agreement between the theoretical and unaveraged data in the region of the primary minimum. The light curves of GY Cnc observed during quiescence are reproduced quite satisfactorily, enabling us to draw some conclusions concerning changes of the disk parameters accompanying brightness variations of the system in the framework of our model. Strong brightness fluctuations can be noted in some of the orbital curves, mainly near the first quadrature, and more rarely near the second quadrature. Note that the data scatter at the quadratures, as well as in other parts of the light curves, was lowest for the JD 7101 and JD 7108 light curves. Panels IV of Figs. 10–13 show the contributions to the combined flux from the system in relative units from the system's components: the (*1*) WD, (*2*) RD, (*3*) disk with the hot spot, and (*4*) hot line. Considering the orbital variations of the components' relative contributions to the combined brightness of the system, we found that the main contribution to the combined flux during these two dates came from the secondary. The contribution of light from the disk was almost a factor of four lower than the mean flux from the star, while the contribution from the hot line was somewhat higher than or comparable to the flux from the disk. A logical conclusion is that the source of the flux fluctuations is instabilities in the radiation from the gas in the interaction region between the stream and the disk and, less importantly, in the disk itself.

Table 5 presents variation ranges for the radiation fluxes from the various components, to facilitate comparison of the light curves for the different data sets.

The following conclusions can be drawn from an analysis of the figures and of Table 5.

1. The light-curve amplitude of GY Cnc in quiescence is mainly determined by the orbital variations of the fluxes from the disk, hot line, and RD in various combinations. The flux from the WD is low due to the star's small size, $F_{\rm wd} \sim 0.044$ rel. units, and has no appreciable influence on the light-curve shape; the same is true for the eclipse of the WD by the body of the secondary.

2. Orbital variations of the flux from the donor F_2 indicate an appreciable role of the ellipsoidal effect in forming the variations; the mean flux from the star is $F_2 \sim 2$–4 rel. units. Changes in the mean radiation flux are due to variations of the secondary's effective temperature in quiescence in the range 3440–3900 K (K8.8 V–M1.7 V [20]). The influence of the reflection effect is not large during quiescence, and is manifest

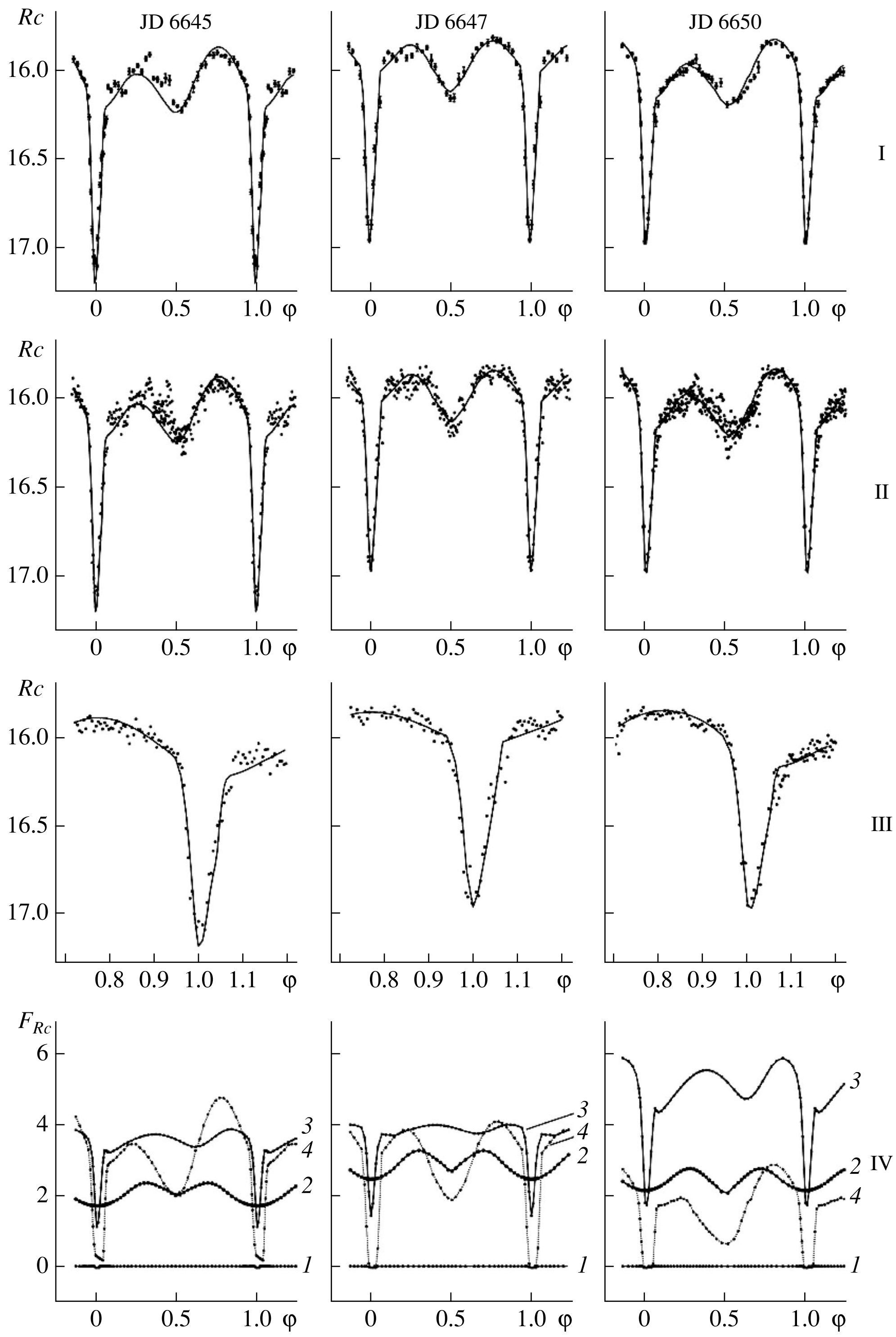

Fig. 10. The results of the solution for the parameters of GY Cnc based on light curves obtained from the data sets for JD 6645, JD 6647, and JD 6650. Top to bottom: the mean light curves (data points with corresponding uncertainties) (I), unaveraged observations (points) folded with the orbital period for the complete orbital cycle (II) and near the primary minimum (III). The solid curve in panels I, II, III is the theoretical synthetic light curve with the parameters from Table 4. The bottom panel (IV) shows the contributions to the combined flux from the (*1*) WD, (*2*) RD, (*3*) accretion disk with the hot spot on its lateral surface, and (*4*) hot line.

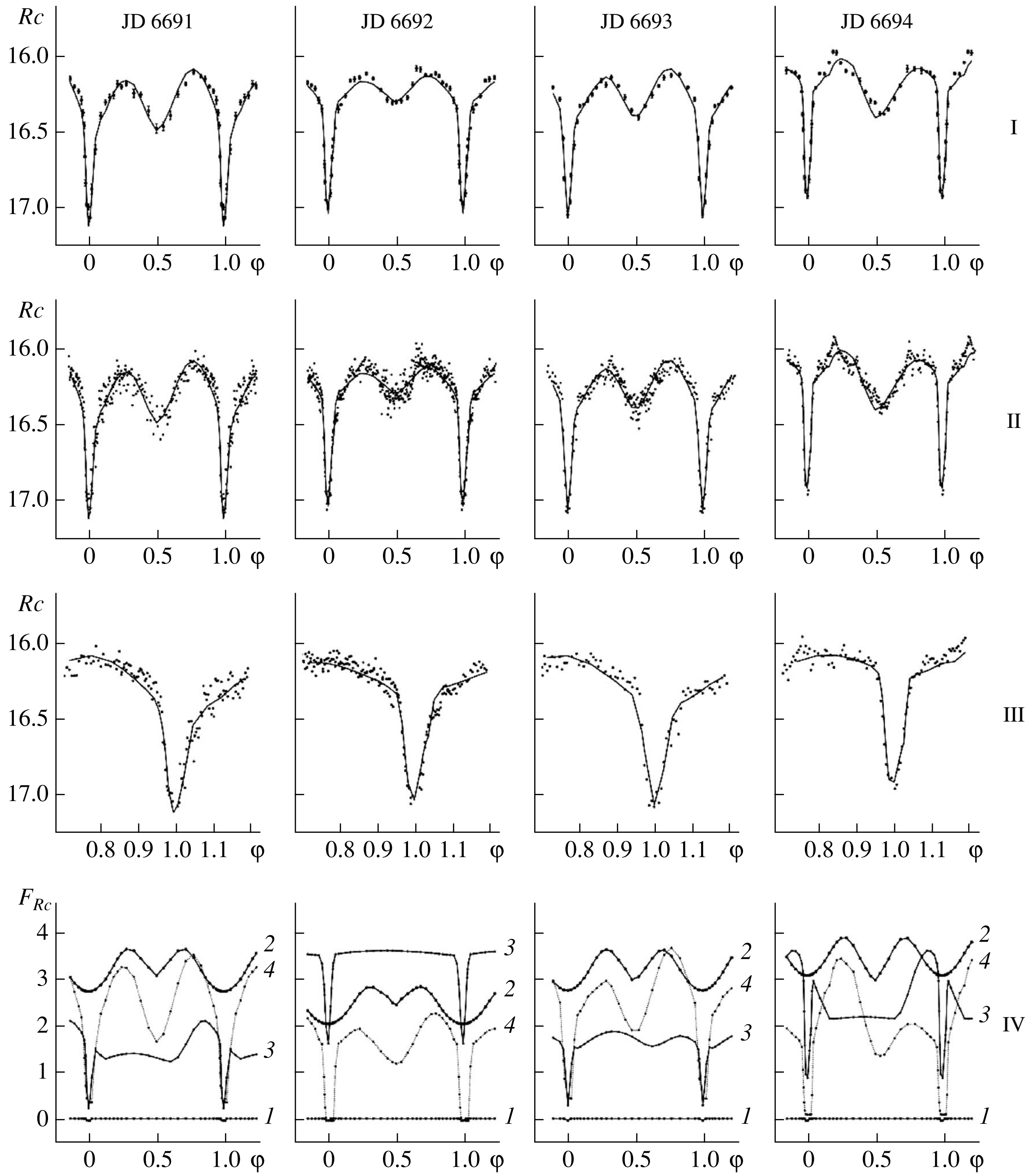

Fig. 11. Same as Fig. 10 for the observations of JD 6691, JD 6692, JD 6693, and JD 6694.

only as a slight increase of the radiation flux in the secondary minimum ($\varphi \sim 0.5$) (see Table 5). In our model, the strength of the reflection effect depends on the temperature of the inner disk regions, $T_{\rm in}$, which varied during our observations within 34 000–42 000 K.

3. Details of the system's out-of-eclipse brightness are determined by the radiation flux from the disk and the hot spot on its lateral surface (curves *3*), and from the hot line (curves *4*). None of the light curves display a total eclipse of the disk (see Table 5). Table 4 shows that, since the disk is fairly elliptical, its maximum radius at apastron ($R_d = a(1+e)$) and minimum radius at periastron ($R_d = a(1-e)$) can differ by a factor of 1.5 for $e = 0.2$. However, such high e values occur only for low semi-major axes a: $a \lesssim 0.2a_0$. The shape of the disk becomes more circular, $e < 0.1$, with increasing a, and its semi-axes become closer to each other. Figure 14 displays the relation of the semi-major axis of the disk a and its eccentricity e in quiescence and during the outburst, as derived from the observations. There is a clear

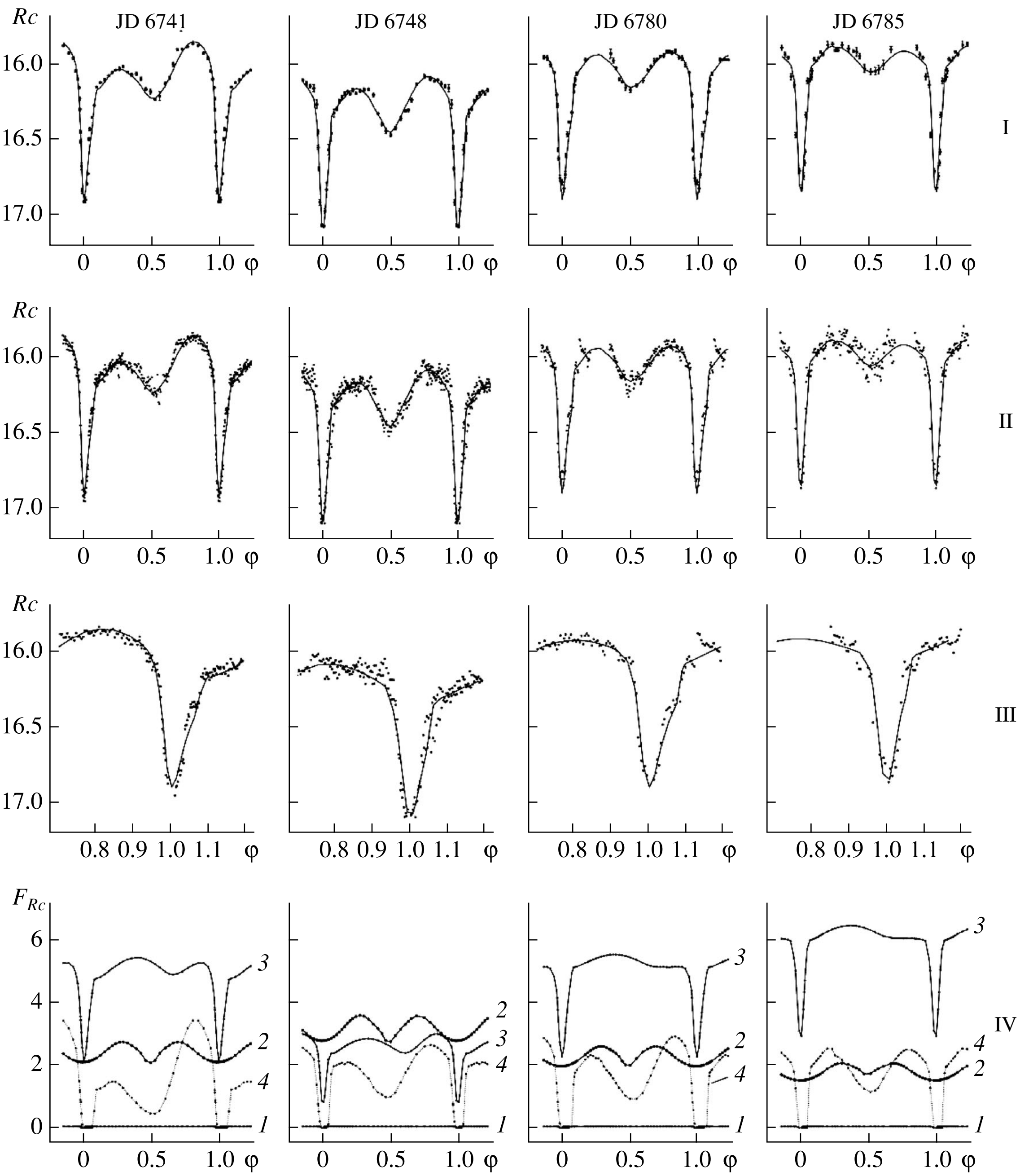

Fig. 12. Same as Fig. 10 for the observations of JD 6741, JD 6748, JD 6780, and JD 6785.

tendency for the disk to become more round with increasing radius.

We did not observe a total eclipse of the accretion disk in any of the light curves, even for the parameter set with the lowest disk radius. This is because the orbital inclination is $i = 73°$, so that even disks with the smallest radii are not totally eclipsed. Figure 15 shows schematics of the GY Cnc system plotted for the parameter sets corresponding to JD 7107 (with the lowest contribution of the light from the disk, at phase $\varphi = 0.0$, $F_\mathrm{d} \sim 0.151$ rel. units), and JD 6785, with the highest flux from the disk ($F_\mathrm{d} \sim 2.942$ rel. units), at a time close to mid-eclipse. We can see that, even for a small disk, almost half its surface is visible to the observer. The radiation flux in the eclipse depends on both the disk radius and luminosity, which is determined by the parameters T_in and α_g. Thus, $a = 0.130a_0$ for the data set for JD 6691, but the temperature of the inner disk regions is higher than for JD 7107, and the radial temperature distribution in the disk is steeper (see Table 4). As a result, the flux

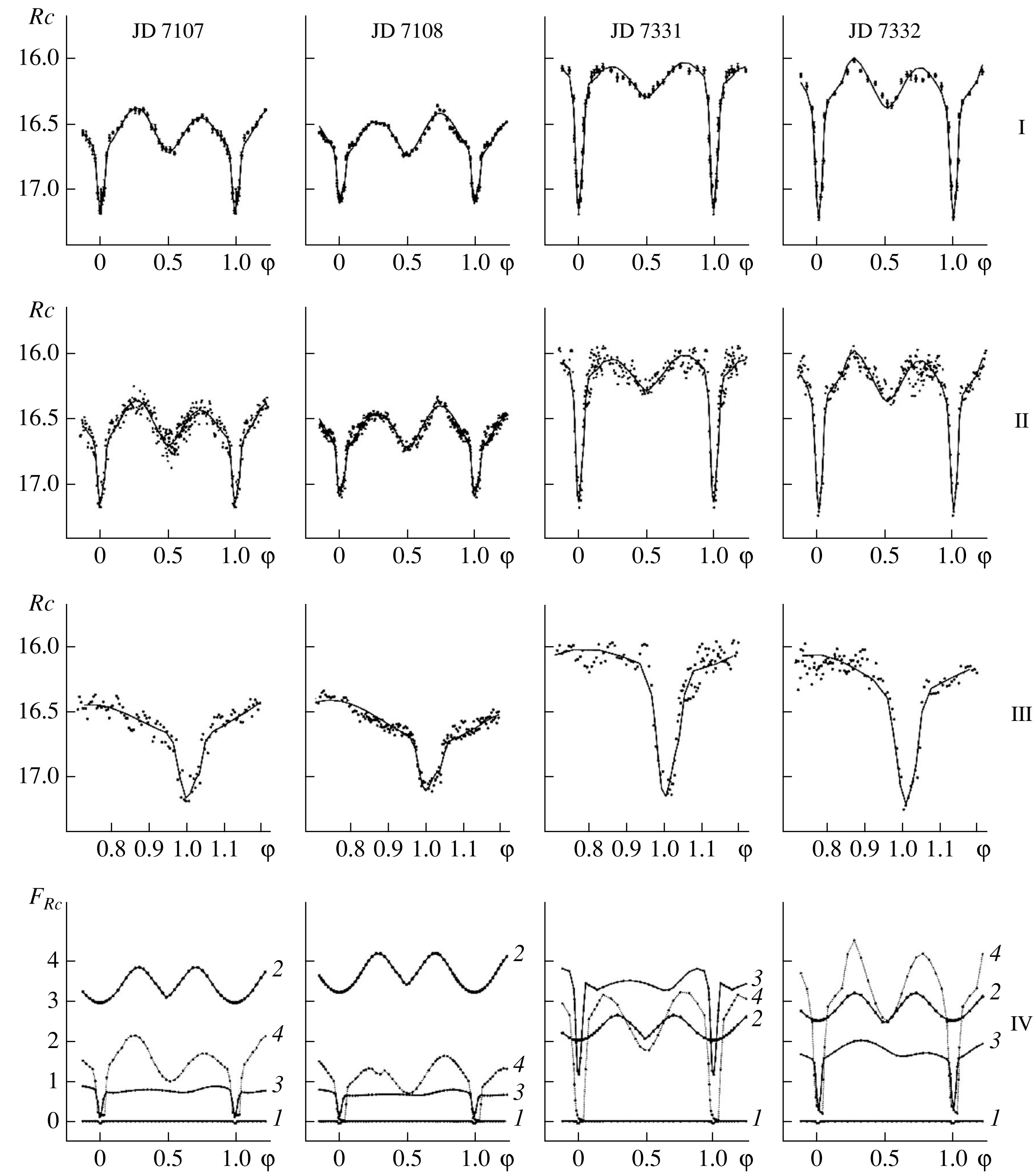

Fig. 13. Same as Fig. 10 for the observations of JD 7107, JD 7108, JD 7331, and JD 7332.

from the disk is almost a factor of two higher during the eclipse, $F_{\rm d} \sim 0.270$ rel. units.

The orbital hump in the light curve is due to the combined contribution of the radiation from the hot spot on the disk surface, light from the leeward side of the hot line and light from the disk at its outer edge. The orbital variation curves for the flux from the disk change strongly from one set of observations to another, and can tentatively be subdivided into two types.

The first visually resembles a classical CV light curve: a deep minimum at $\varphi \sim 0$, a pre-eclipse hump, and smooth out-of-eclipse variations. The second type corresponds to a light curve without a pre-eclipse hump (JD 6692, JD 6780, JD 6785, JD 7332); variations of the out-of-eclipse brightness can be completely absent (JD 6692), or may display a wave at phases $\varphi \sim 0.3{-}0.5$. The presence of such a wave and its characteristics (amplitude, orbital phase of its maximum, etc.) are due to the combined action of the eccentricity, radius, luminosity, and periastron azimuth of the disk.

Table 5. Fluxes in relative units for the GY Cnc components in 2013–2015 derived from the solution for the system parameters obtained using the "combined" model

Parameter	JD 6645	6647	6650	6691	6692	6693	6694	6741	6748
Red dwarf									
Min $\varphi = 0.0$	1.747	2.497	2.184	2.783	2.084	2.808	3.130	2.105	2.792
Phase $\varphi = 0.5$	2.050	2.718	2.116	3.123	2.496	3.039	3.027	2.081	2.761
Quadratures	2.396	3.306	2.790	3.692	2.885	3.687	3.937	2.754	3.592
White dwarf									
Min $\varphi = 0.0$	0.0	0.0	0.0	0.0	0.0	0.0	0.0	0.0	0.0
Max	0.044	0.044	0.044	0.044	0.044	0.044	0.044	0.044	0.044
Accretion disk									
Min $\varphi = 0.0$	1.288	1.471	1.764	0.270	1.664	0.331	0.920	2.147	0.822
$\varphi \sim 0.1-0.6$	3.75	3.39	5.55	1.40	3.60	1.85[2]	2.23	5.18[2]	2.65[2]
Hump	3.911	4.038	5.919	2.148	3.59[1]	1.826	3.658	5.272	3.002
Hot line									
Min $\varphi \sim 0.0$	0.209	0.0	0.0	0.402	0.0	0.502	0.133	0.0	0.0
Max $\varphi \sim 0.2$	3.486	3.897	1.981	3.305	1.980	3.012	3.490	1.480	2.102
Max $\varphi \sim 0.8$	4.789	4.124	2.897	3.575	2.308	3.722	2.081	3.427	2.657

Parameter	**JD 6762**	**6764**	**6768**	**6769**	6780	6785	7107	7108	7331	7332
Red dwarf										
Min $\varphi = 0.0$	**0.335**	**0.252**	**0.988**	**2.514**	1.972	1.517	3.003	3.267	2.068	2.556
Phase $\varphi = 0.5$	**17.18**	**4.838**	**1.309**	**2.491**	2.004	1.732	3.141	3.463	2.106	2.522
Quadratures	**5.800**	**1.600**	**1.454**	**3.226**	2.609	2.065	3.890	4.240	2.695	3.248
White dwarf										
Min $\varphi = 0.0$	**0.0**	**0.0**	**0.0**	**0.0**	0.0	0.0	0.0	0.0	0.0	0.0
Max	**0.044**	**0.044**	**0.044**	**0.044**	0.044	0.044	0.044	0.044	0.044	0.044
Accretion disk										
Min $\varphi = 0.0$	**40.69**	**8.567**	**1.984**	**1.307**	2.281	2.942	0.151	0.172	1.208	0.334
$\varphi \sim 0.1-0.6$	**119**[1]	**35.30**	**5.60**[2]	**4.36**[2]	5.35[2]	6.28[2]	0.80	0.71	3.44[2]	1.87[2]
Hump	**109**	**33.6**[1]	**5.40**[1]	**4.768**	5.15[1]	6.07[1]	0.92	0.83	3.856	1.66[1]
Hot line										
Min $\varphi \sim 0.0$	**0.0**	**0.0**	**0.495**	**0.175**	0.0	0.0	0.195	0.055	0.110	0.238
Max $\varphi \sim 0.2$	**29.54**	**29.65**	**4.775**	**4.076**	2.334	2.542	2.180	1.367	3.204	4.568
Max $\varphi \sim 0.8$	**31.70**	**28.42**	**5.433**	**5.487**	2.926	2.502	1.736	1.680	3.271	4.235

For quiescent dates, the "quadratures" correspond to the phases of highest brightness of the secondary; for outburst dates, they correspond to phases $\varphi = 0.25$ and 0.75. Data for outburst dates are in bold face.

[1] The pre-eclipse hump is missing.

[2] Instead of a plateau, there is a wave with a maximum at $\varphi \sim 0.3-0.4$.

4. Finally, the light curve of the hot line has a classical shape with two maxima, at phases $\varphi \sim 0.2$ and 0.8, when the emitting regions of the hot line are in the line of sight. As a rule, due to its better visibility, the hump on the leeward side ($\varphi \sim 0.8$) is higher than the hump on the windward side, despite the higher temperature of the latter. It follows from Table 5 that the contribution from the hot line is 2–4 rel. units,

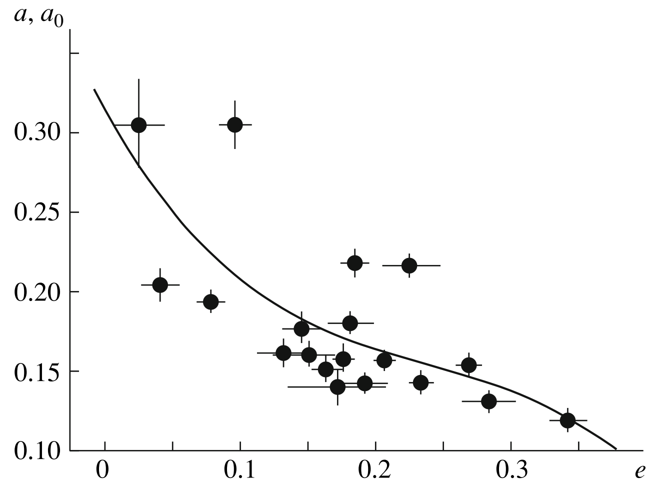

Fig. 14. Relation between the semi-major axis of the accretion disk, a, and its eccentricity, e, obtained from the solution for the light curves of GY Cnc. The solid curve approximates the observations using a third-order polynomial.

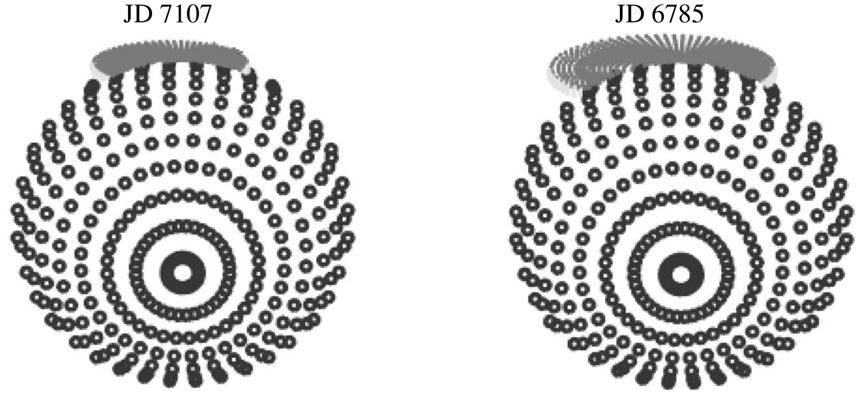

Fig. 15. Schematic views of GY Cnc near mid-eclipse plotted for the set of parameters corresponding to JD 7107 and JD 6785, with the minimum and maximum radiation flux from the disk.

and varies less than the contribution of the disk to the combined flux.

7.2. Light Curves During the Outburst

The outburst parameters of the components of GY Cnc are presented in Table 4. The theoretical light curves plotted with the tabulated parameters are shown and compared to the observed light curves in Fig. 16, which is plotted using the same scheme as Figs. 10–13. We can see that the system has almost returned to quiescence by JD 6768, though the brightness fluctuations during JD 6769 were quite large.

The origin of the observed outburst was an abrupt increase in the disk luminosity, to ~120 rel. units on JD 6762 and to ~35 rel. units on JD 6764, due to an increase of the temperature $T_{\rm in}$ and a decrease of α_g to ~0.1–0.2. A similar effect has also been observed in other studies (e.g., [21]). The disk radius at the outburst maximum was $a \sim 0.143a_0$; this radius was smallest two days after the maximum, $a \sim 0.119a_0$, possibly indicating an efficient infall of matter onto the WD surface during the development of the outburst. The WD temperature was fixed in our computations, but a possible increase, at least in the orbital plane, is indicated by the increase of the matter temperature in the first orbit in the disk near the WD surface to ~95 000 K; in quiescence, this temperature parameter did not exceed ~43 000 K.

The secondary's light curve is characterized by a strong reflection effect, to ~17 rel. units near the ellipsoidal minimum at $\varphi \sim 0.5$, due to strong heating of the star by its companion. Two days after the outburst maximum, the temperature of the inner disk parts was still high, $T_{\rm in} \sim 68\,000$ K, and the reflection effect was significant, reaching 5 rel. units at $\varphi \sim 0.5$. The matter at the base of the hot line was similarly

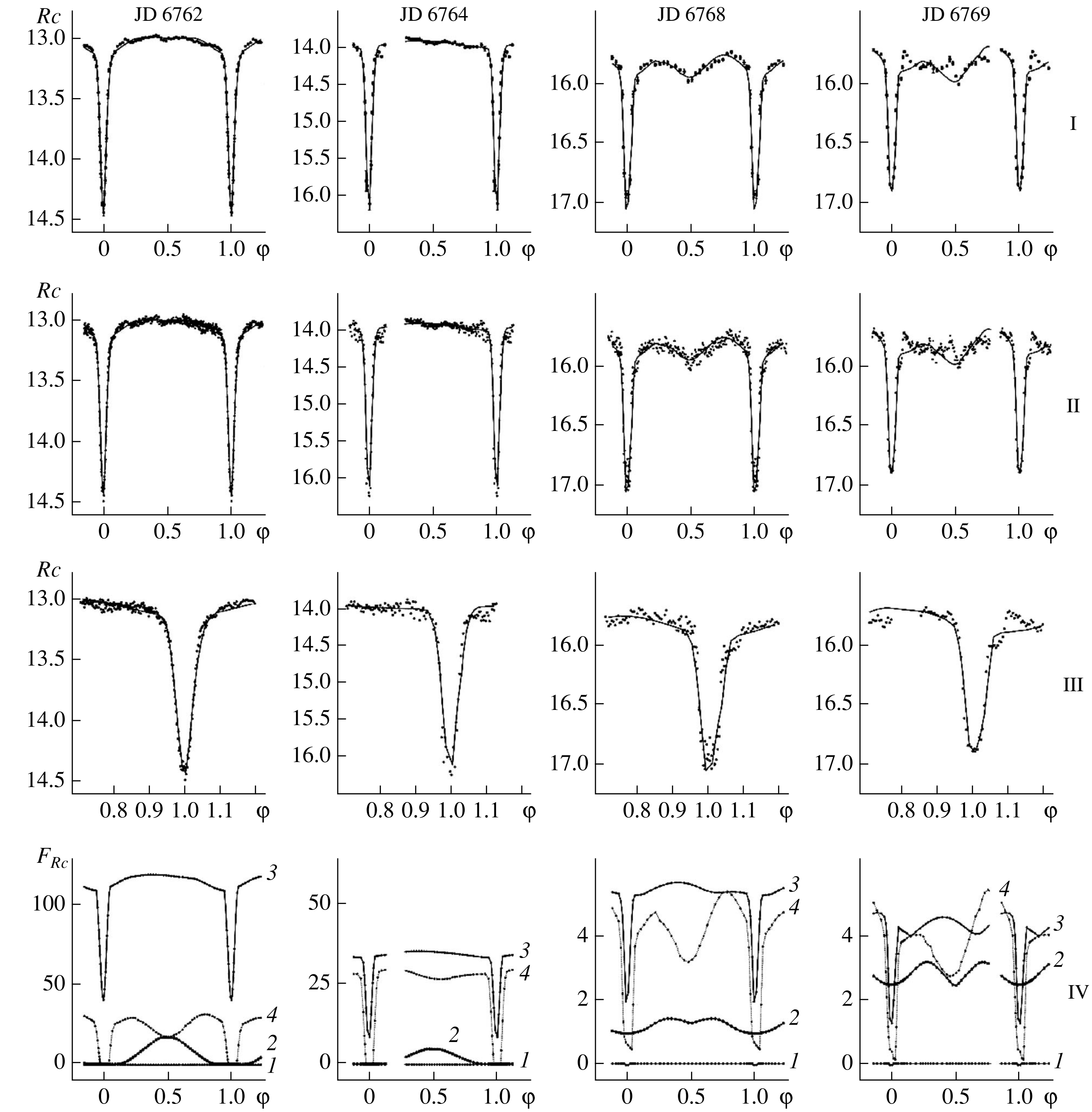

Fig. 16. Same as Fig. 10 for observations during the outburst, on JD 6762, JD 6764, JD 6768, and JD 6769.

strongly heated; its contribution to the combined flux is a factor of 10–15 higher than the luminosity of the base of the stream in quiescence (see Table 5).

8. DISCUSSION

Figure 17 shows the main parameters of the accretion disk versus time, based on the data from Fig. 4. The uncertainties of the parameters are, on average, within the size of the data points, with the exception of the secondary's temperature near the outburst maximum. The area within the vertical lines corresponds to the April 2014 outburst; the data points in this area are plotted gray. The during the outburst are given to enable a comparison of the corresponding parameters before, during, and immediately after the outburst.

All the parameters displayed in the figure demonstrate more or less significant variations even within one to two days. This is especially evident for the sequence of light curves obtained on the four nights of JD 6691–6694. The dispersion of the parameters for the time interval of the observations (∼700 days) is comparable to that found for two to five days.

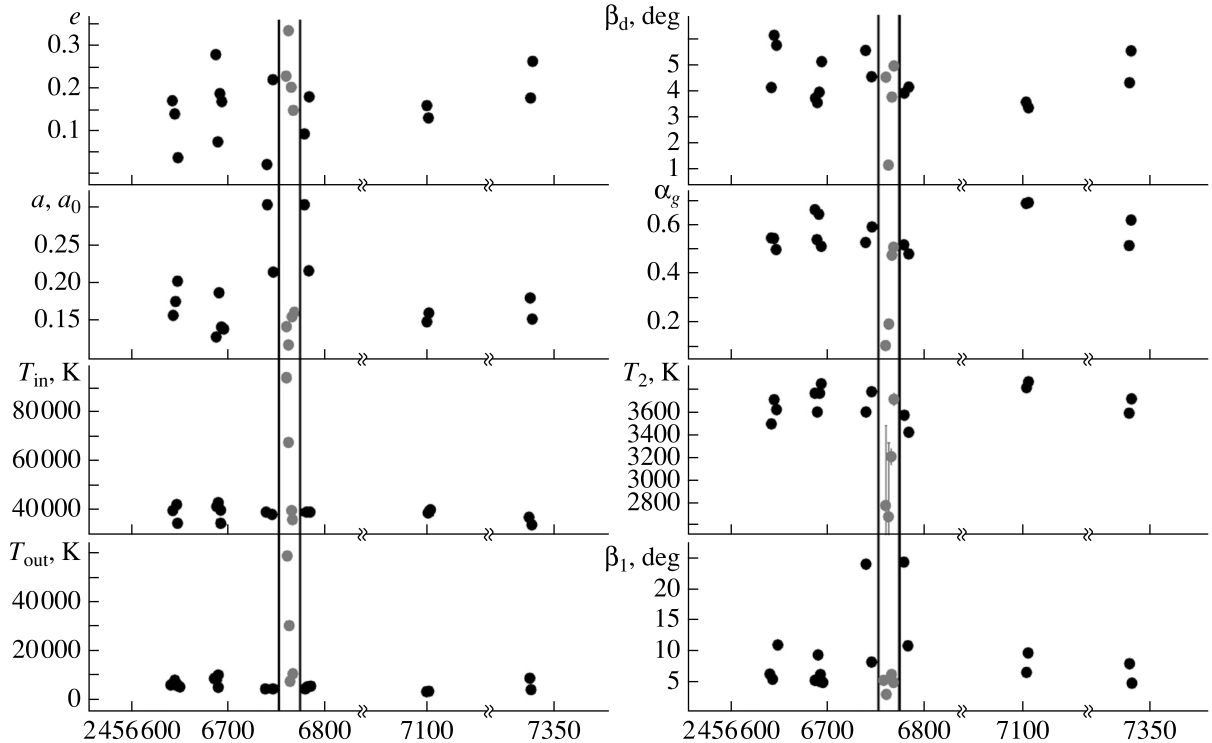

Fig. 17. Parameters of the GY Cnc accretion disk versus time: eccentricity e, semi-major axis a, gas temperature in the inner parts of the disk $T_{\rm in}$ and at its outer edge $T_{\rm out}$, the total thickness of the outer edge of the disk $\beta_{\rm d}$, in degrees, α_g, the temperature of the secondary T_2, and the angle between the axis of the gas stream and the line joining the component centers of mass β_1, in degrees. The vertical lines indicate the outburst region, and gray circles show the corresponding parameters derived during the outburst. The mean uncertainties of the parameters are close to the size of the data points.

Let us compare the behavior of the components' parameters during the outburst and neighboring time intervals. The semi-major axis of the elliptical disk is largest prior to and just after the outburst: $a \sim 0.2{-}0.3a_0$ two weeks before and after the outburst, and decreases to $a \sim 0.12a_0$ during the outburst, accompanied by an increase of the disk eccentricity to $e \sim 0.34$. At other times, a varies in the range $a/a_0 \sim 0.13{-}0.30$.

The temperatures of the matter near the WD ($T_{\rm in}$) and at the outer edge of the disk ($T_{\rm out}$) before and after the outburst are 38 000–39 000 K and ~4700 K, respectively, close to the mean values of these parameters in quiescence.

The total thickness of the outer edge of the disk varies within $\beta_{\rm d} \sim 3^\circ{-}6^\circ$ both in quiescence and during the outburst. Only two days after the outburst maximum, $\beta_{\rm d}$ decreased to 1°, providing evidence, together with the small disk radius at this time, for a considerable decrease in the amount of matter in the disk.

The parameter α_g varies within 0.5–0.65 in quiescence. Its value approached $\alpha_g \sim 0.7$ on only two dates, JD 7107 and JD 7108. Recall that it is assumed that each particle in the disk emits as a blackbody for $\alpha_g = 0.75$, and that the radial distribution of the temperature in the disk is the steepest. As a result, the disk's contribution to the combined flux from the system is lowest for these two nights, compared to the other data sets. Just before the outburst, $\alpha_g \sim 0.6$, while $\alpha_g \sim 0.53$ just after the outburst. At the outburst maximum, α_g decreases to ~0.1, then smoothly changes from $\alpha_g \sim 0.2$ to ~0.48–0.50 as the outburst develops.

Thus, we can conclude that the re-adjustment of the disk's internal characteristics that resulted in the outburst occurred at a time $\Delta t < 10^d$ before its maximum.

The behavior of the secondary's effective temperature is of interest. In quiescence, it varies between 3400 and 3900 K, corresponding to spectral types K8.8 V–M1.7 V. The lower limit for the spectral type of the secondary we have derived is close to the upper limit presented in [6], M3 ± 1.5 V, which was derived from a comparison of the TiO/CaOH ($\lambda\lambda$ 6160–6320 Å) and TiO ($\lambda\lambda$ 7190–7210 Å) bands with data from a catalog of observed M-dwarf spectra. Unfortunately, conclusions on the spectral type of GY Cnc were based on only one available spectrum [6]. The star's calculated effective temperatures for the outburst maximum decreased to 2600–2700 K. However, due to the very strong reflection effect, the uncertainty in these values is quite high, $\Delta T_2 \sim 700$ K, comparable to the deviation of T_2 on these nights from the mean quiescence value.

The eighth panel of the figure displays variations of the angle between the axis of the gas stream and the system's axis β_1. This parameter can be considered an indicator of the rate of matter outflow from the RD: the larger this angle, the lower the velocity of matter in the gas stream. On average, β_1 varies within $\beta_1 \sim 5°{-}11°$. It decreased to $\beta_1 \sim 3°{-}6°$ during the outburst; i.e., the outflow rate was above its average value. The outflow rate from the secondary was lower 21 days before (JD 6741) and 11 days after (JD 6780) the outburst, with this parameter reaching $\beta_1 \sim 24°{-}25°$. On JD 6748 (14 days before the outburst maximum), the parameter was $\beta_1 \sim 8°{-}9°$. Unfortunately, we have too few data for any definite conclusions, and can only assert that the rate of matter outflow from the secondary varies.

Let us now compare the system parameters we obtained to those derived earlier from studies of the eclipse shape (see Table 1). We were able to construct theoretical light curves that are consistent with all 19 observed curves obtained over $\sim 700^d$ with the basic parameters of the system $q = 1.9(2)$, $i = 73.0(4)°$, $T_{\rm wd} = 18\,000 \pm 400$ K, $R_{\rm wd}/a_0 = 0.0040(7)$, and $R_2/a_0 = 0.335(7)$. The component mass ratio, q, and WD radius, $R_{\rm wd}/a_0$, we derived lie within the range of parameters obtained in [2], but are much lower than those for the solution of Thorstensen [7]. Our orbital inclination was $\sim 3°$ lower than the value obtained in [2] for $q \sim 2.0$. This may be due to our model, which included light from the hot line. Our WD temperature was also lower than the value found in [2], but the difference of 1500–2000 K is insignificant due to the star's small radius. Using the same technique as that applied in [2] to determine the component masses and separation a_0, we found $M_{\rm wd} = 0.73(7) M_\odot$, $M_2 = 0.386(3) M_\odot$, and $a_0 = 1.37(3) R_\odot$. We then find for this value of a_0 and the values of $R_{\rm wd}/a_0$ and R_2/a_0 from Table 4 $R_{\rm wd}/R_\odot = 0.0055 \pm 0.0011$ and $R_2/R_\odot = 0.459 \pm 0.021$. Both values are in the ranges obtained in [2].

9. CONCLUSIONS

We summarize the main results of our study below.

1. We have obtained photometric observations of the dwarf nova GY Cnc in the near infrared (the Rc filter) in 2013–2015. Our observations cover a total of ~700 days (~3900 orbital cycles) and were subdivided into three groups: from December 2013 to May 2014 (JD 2456645–6785), two nights in March 2015 (JD 2457107–7108), and two nights in November 2015 (JD 2457331–7332). The first group includes an outburst in April 2014, while the other observations correspond to the brightness level of system's quiescence.

2. We used the numerous new photometric data in quiescence to search for an orbital period valid in 2013–2015. Within the uncertainties, the resulting $P_{\rm orb}$ value coincides with the periods determined in 2000–2002 (see Table 3). The phased light curves of the system exhibit appreciable variations of their shapes and magnitudes in the eclipse minimum in the range $16.8{-}17.2^m$. The total variation amplitude varies from 0.8^m to 1.2^m, with the lower amplitudes being due to lower out-of-eclipse brightness levels of the system, with the eclipse magnitude remaining at the level $17.1{-}17.2^m$ (JD 2457107–7108). The orbital hump is missing for some of the light curves.

3. We determined the parameters of the components of the GY Cnc system using a "combined" model for a cataclysmic variable taking into account the fluxes from both the hot line and a hot spot on the leeward side of the stream. An obvious advantage of this model is that it makes it possible to analyze the *complete* light curve and not only the region of the eclipse.

4. The mean temperature of the red dwarf, $T_2 \sim 3667$ K (M0.2 V [20]), it varies from 3440 to 3900 K (K8.8–M1.7 V). The effective temperature can change by ~150–200 K within one to two days ($(5{-}12) P_{\rm orb}$). Such variations could be due, among other reasons, to changes in the heating of the star by radiation from inner parts of the disk.

5. On average, the accretion disk is smaller than the size derived earlier in the parametric model of the eclipse profile [2, 6]. The disk has a considerable eccentricity when its semi-major axis a is small, $a \lesssim 0.2a_0$. With increasing a, the disk shape becomes more circular, $e < 0.1$. For the orbital inclination $i = 73°$, no total eclipse of the accretion disk is observed for any of the light curves, even for the set of parameters with the smallest disk radius.

6. The outburst of the cataclysmic variable GY Cnc was due to an abrupt increase in the disk luminosity, by at least a factor of ~30, due to a decrease in the parameter α_g to ~0.1–0.2 and an increase in the temperature $T_{\rm in}$ to ~95 000 K. In quiescence, $T_{\rm in} \lesssim 43\,000$ K. The reason for the temperature increase near the WD surface could be a strong infall of matter on its surface during the development of the outburst: the disk radius was the smallest, $a \sim 0.119 a_0$, on the second day after maximum (i.e., after $\sim 11 P_{\rm orb}$).

7. Considerable variations about their mean values are typical for all the parameters of the accretion disk in quiescence: $\Delta a/a_0 \sim 40\%$, $\Delta e \sim 75\%$, $\Delta T_{\rm in} \sim$

10%, $\Delta T_{\rm out} \sim 48\%$, and $\Delta \alpha_g \sim 18\%$. Out-of-outburst variations of the disk parameters have also been observed for other cataclysmic variables [11, 22].

ACKNOWLEDGMENTS

This study was supported by the Russian Foundation for Basic Research (project no. 14-02-00825) and by the Program of State Support to Leading Scientific Schools of the Russian Federation (grant no. NSh-1675.2014.2).

REFERENCES

1. B. Warner, *Cataclysmic Variable Stars* (Cambridge Univ. Press, Cambridge, 1995).
2. A. W. Shafter, L. L. Clark, J. Holland, and S. J. Williams, Publ. Astron. Soc. Pacif. **112**, 1467 (2000).
3. H. J. Hagen, D. Groote, D. Engels, and D. Reimers, Astron. Astrophys. Suppl. Ser. **111**, 195 (1995).
4. W. Voges, B. Aschenbach, Th. Boller, H. Bräuninger, U. Briel, W. Burkert, K. Dennerl, J. Englhauser, R. Gruber, F. Haberl, G. Hartner, G. Hasinger, M. Kürster, E. Pfeffermann, W. Pietsch et. al, Astron. Astrophys. **349**, 389 (1999).
5. N. Bade, D. Engels, W. Voges, V. Beckmann, Th. Boller, L. Cordis, M. Dahlem, J. Englhauser, K. Molthagen, P. Nass, J. Studt, and D. Reimers, Astron. Astrophys. Suppl. Ser. **127**, 145 (1998).
6. B. T. Gänsicke, R. E. Fried, H.-J. Hagen, K. Beuermann, D. Engels, F. V. Hessman, D. Nogami, and K. Reinsch, Astron. Astrophys. **356**, L79 (2000).
7. J. R. Thorstensen, Publ. Astron. Soc. Pacif. **112**, 1269 (2000).
8. T. Kato, R. Ishioka, and M. Uemura, Publ. Astron. Soc. Jpn. **54**, 1023 (2002).
9. S. Yu. Shugarov, N. A. Katysheva, and P. Kroll, in *Stellar Variability, Proceedings of the AFOEV International Conference on Variable Stars, Bourbon-Lancy, France, August 26–28, 2002* (Burillier, Vannes, 2003), p. 95.
10. W. J. Feline, V. S. Dhillon, T. R. Marsh, C. A. Watson, and S. P. Littlefair, Mon. Not. R. Astron. Soc. **364**, 1158 (2005).
11. T. S. Khruzina and I. B. Voloshina, Astron. Rep. **59**, 366 (2015).
12. T. S. Khruzina, Astron. Rep. **42**, 180 (1998).
13. T. S. Khruzina, Astron. Rep. **55**, 425 (2011).
14. N. I. Shakura and R. A. Sunyaev, Astron. Astrophys. **24**, 337 (1973).
15. D. V. Bisikalo, A. A. Boyarchuk, P. V. Kaigorodov, and O. A. Kuznetsov, Astron. Rep. **47**, 809 (2003).
16. D. V. Bisikalo, A. A. Boyarchuk, O. A. Kuznetsov, and V. M. Chechetkin, Astron. Rep. **41**, 720 (1997).
17. D. Himmelblau, *Applied Nonlinear Programming* (McGraw-Hill, New York, 1972; Mir, Moscow, 1975), p. 163.
18. T. S. Khruzina, A. M. Cherepashchuk, D. V. Bisikalo, A. A. Boyarchuk, and O. A. Kuznetsov, Astron. Rep. **47**, 214 (2003).
19. I. B. Voloshina and T. S. Khruzina, Astron. Rep. **56**, 819 (2012).
20. G. M. H. J. Habets and J. R. W. Heintze, Astron. Astrophys. Suppl. Ser. **46**, 193 (1981).
21. G. Djurasevic, Astrophys. Space Sci. **240**, 317 (1996).
22. T. S. Khruzina, P. Yu. Golysheva, N. A. Katysheva, S. Yu. Shugarov, and N. I. Shakura, Astron. Rep. **59**, 288 (2015).

Translated by N. Samus'